AD-A073 006 UNITED TECHNOLOGIES RESEARCH CENTER EAST HARTFORD CONN F/G 20/4
AN EXPERIMENTAL AND ANALYTICAL STUDY OF BOUNDARY LAYERS IN HIGH--ETC(U)
JUL 79 M F BLAIR F49620-78-C-0064
UNCLASSIFIED UTRC/R78-914388-5 AFOSR-TR-79-0936 NL

| OF |
AD
A073006

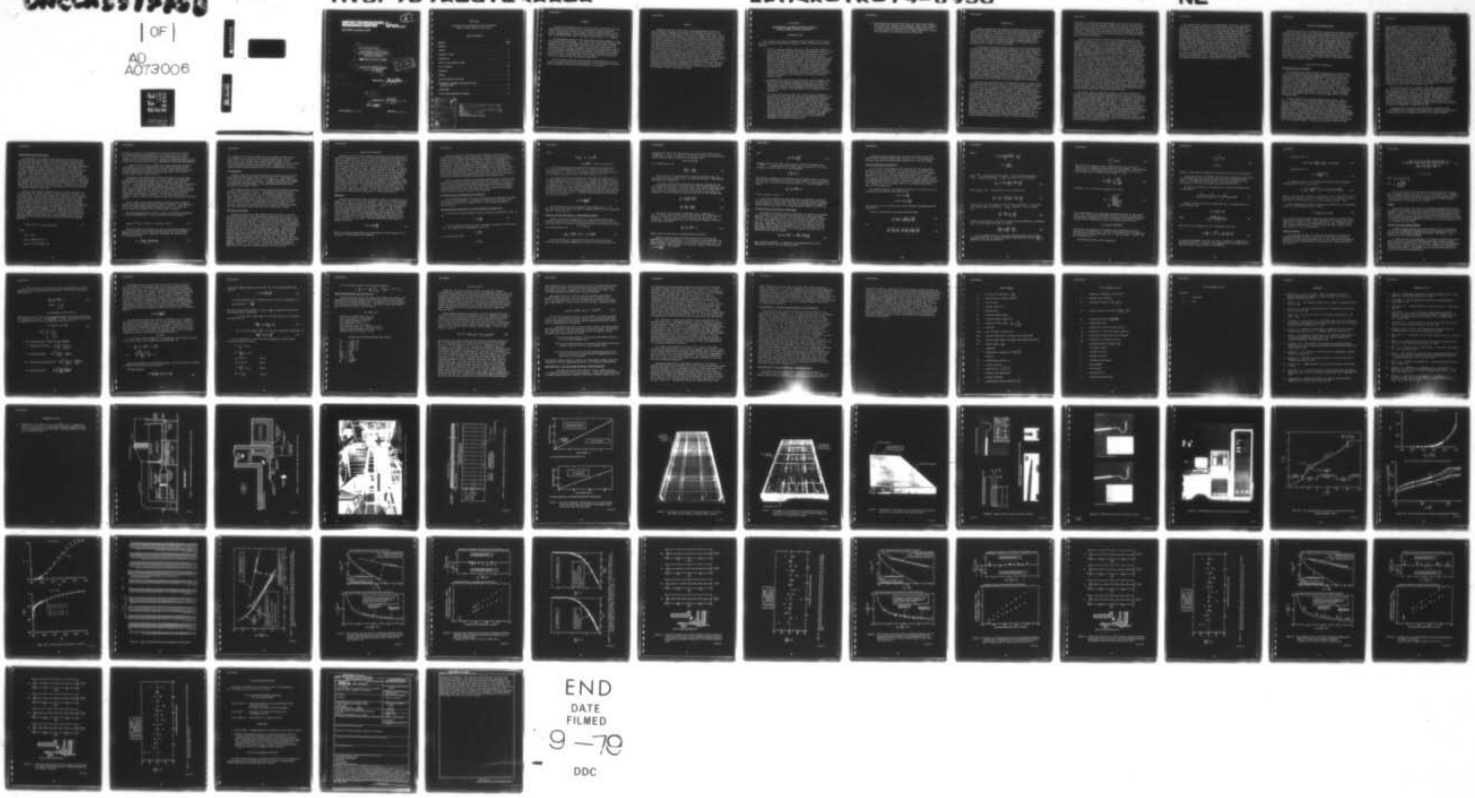

END
DATE
FILMED
9-79
DDC

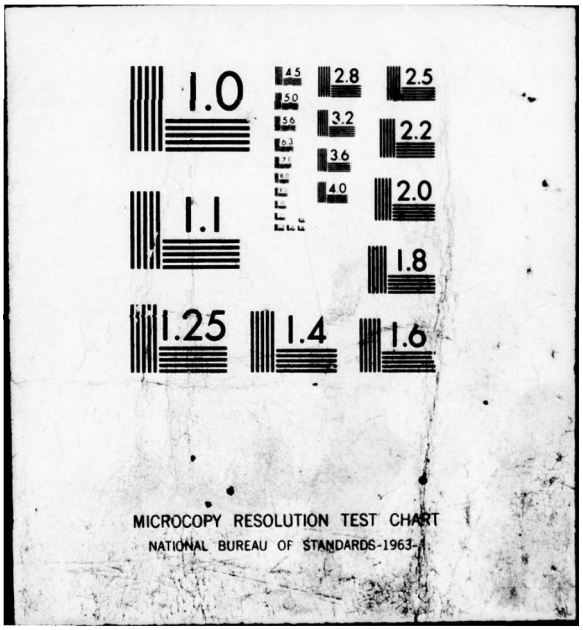
1.0
1.1
1.25
1.4
1.6
1.8
2.0
2.2
2.5
2.8
3.2
3.6
4.0
4.5
5.0
5.6
MICROCOPY RESOLUTION TEST CHART
NATIONAL BUREAU OF STANDARDS-1963-A

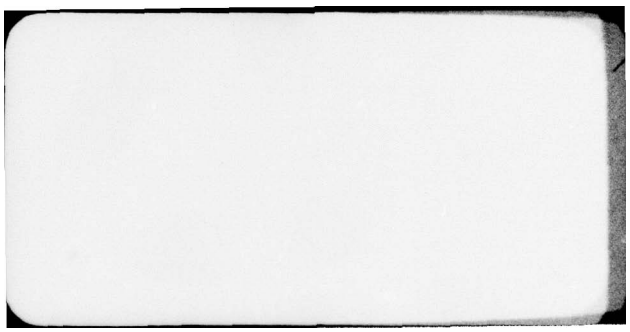

(6)

UNITED TECHNOLOGIES RESEARCH CENTER

UNITED TECHNOLOGIES

East Hartford, Connecticut 06108

(14) UTRC/R78-914388-5

(6) An Experimental and Analytical Study of Boundary Layers in Highly Turbulent Freestreams.

(9) ~~Final~~ Annual Scientific Report no. 1

1 Jun 78 - 1 Jun 79

(15) Contract No. F49620-78-C-0064

Project-Task 2307/A4

61102 F

(16) (17)

(15) AFOSR

(19) TR-79-D936

REPORTED BY M. F. Blair

M. F. Blair

(10)

(12) 73 p.

APPROVED BY MJ Werle

M. J. Werle

(11)

DATE Jul~~y~~ 1979

NO. OF PAGES _____

COPY NO. _____

409 252

R78-914388

An Experimental and Analytical Study of Boundary Layers in Highly Turbulent Freestreams

TABLE OF CONTENTS

FOREWORD

This report was prepared for the Air Force Office of Scientific Research, United States Air Force by the United Technologies Corporation Research Center, East Hartford, Connecticut, under Contract F49620-78-C-0064, Project-Task No. 2307/A4 61102 F. The performance period covered by this report was from 1 June 1978 to 1 June 1979. The project monitor was Dr. D. G. Samaras.

The experimental portions of the investigation are being conducted in the UTRC Boundary Layer Wind Tunnel. This facility was constructed during 1977 and underwent a series of flow quality evaluation tests during 1978. The UTRC Uniform Heat Flux Flat Wall Model, was also constructed, instrumented, and tested during 1978. Finally, a computer controlled data acquisition system for the UTRC Boundary Layer Wind Tunnel was designed, constructed and made operational during 1978. The construction and evaluation testing of the Boundary Layer Wind Tunnel, Uniform Heat Flux Flat Wall Model, and Data Acquisition system were conducted under UTC Corporate sponsorship.

Contract funded efforts have been devoted to the development of a data analysis software package and to the measurement of the heat transfer distributions and boundary layer profile data presented in this report.

ABSTRACT

During the first year of the contract period experimental research has been conducted to determine the influence of free-stream turbulence on zero pressure gradient, incompressible, fully turbulent boundary layer flow. During this period convective heat transfer coefficients, boundary layer mean velocity and temperature profile and wall static pressure distribution data were obtained for two flow conditions of constant free-stream velocity and low free-stream turbulence intensity and for one flow condition of constant free-stream velocity and higher free-stream turbulence. Documentation of the free-stream turbulence for these flows is currently in progress. The conclusion reached from the low free-stream turbulence test results is that these data are in excellent agreement with classic two-dimensional, low free-stream turbulence, turbulent boundary layer correlations, thus establishing the absolute accuracy of the experiment. The data obtained for the higher free-stream turbulence test case indicates that free-stream turbulence does have a significant effect on fully turbulent boundary layer skin friction and heat transfer. A quantitative assessment of this influence will emerge as data is obtained for additional free-stream turbulence levels and as the turbulence distributions are documented. The data obtained during this first year of the contract effort constitute part of task "a" of the Statement of Work of the subject contract.

R78-914388-5

An Experimental and Analytical Study of Boundary Layers in Highly Turbulent Freestreams

STATEMENT OF WORK

The contractor shall furnish scientific effort, together with all related services, facilities, supplies and materials, needed to conduct the following research:

a. For fully turbulent boundary layer flow, convective heat transfer coefficients, boundary layer mean velocity and temperature profiles, wall static pressure distributions, and free-stream turbulence intensity, spectral, and longitudinal integral scale distributions shall be measured using the Contractor's instrumented flat wall installed in the Contractor's Boundary Layer Wind Tunnel. These data shall be obtained with a free-stream turbulence intensity level below 1 percent for two constant free-stream velocities and for three free-stream turbulence levels greater than 1 percent for one constant freestream velocity (a total of five flow conditions). From these data the integral properties (momentum, displacement, and enthalpy thickness) of the boundary layers will be calculated, and, where applicable, the profile data will be reduced to the "universal" coordinates for turbulent boundary layers.

b. The measured heat transfer distributions and turbulent boundary layer profile data obtained under paragraph a above shall be compared to predictions of the UTRC Finite-Difference Boundary Layer deck. The free-stream turbulence energy entrainment calculation procedure currently incorporated in the UTRC deck will be evaluated using these comparisons.

c. For transitional boundary layer flow, convective heat transfer coefficients, boundary layer mean velocity and temperature profiles, wall static pressure distributions, and free-stream turbulence intensity, spectral, and longitudinal integral scale distributions shall be measured using the Contractor's instrumented flat wall installed in the Contractor's Boundary Layer Wind Tunnel. These data shall be obtained for two free-stream acceleration levels with two free-stream turbulence levels each for a total of four flow conditions. From these data, the integral properties (momentum, displacement, and enthalpy thickness) of the boundary layers will be calculated, and, where applicable, the profile data will be reduced to the "universal" coordinates for turbulent boundary layers.

d. The measured heat transfer distributions and transitional boundary layer profile data obtained under paragraph c above shall be compared to predictions of the UTRC Finite-Difference Boundary Layer deck. The method employed in the UTRC deck to compute transitional boundary layer flows will be evaluated using these comparisons.

INTRODUCTION

Improved techniques for calculating heat transfer coefficient distributions on gas turbine airfoils have been sought by engine manufacturers for the entire history of the industry. These heat transfer distributions must be known so that cooling schemes can be tailored to produce the required metal temperature. Accurate heat transfer predictions are an essential feature of gas turbine design because of the need to maximize performance through minimal use of cooling air and the need to minimize development costs through provision of adequate airfoil cooling on the initial design.

In the design of an airfoil cooling scheme the lack of any required heat transfer distribution information may be compensated for by simply overcooling the component. This overcooling may easily exist since gas turbine thermal design systems are typically not based on fundamental fluid mechanics and heat transfer data and analysis alone but rather are calibrated, or adjusted, to provide agreement with engine experience. Among the more obvious benefits that result from elimination of overcooling are reduced aerodynamic cooling penalties, increased burner and turbine mainstream mass flow rates (i.e., increased power) and potentially reduced cost for the fabrication of the airfoil cooling scheme. Furthermore, without a more complete first-principles understanding there is the likelihood that a designer will unknowingly go beyond the range of validity of the design system calibration. There is, then, a clear requirement for the development of airfoil heat transfer distribution prediction procedures which are based on fundamental fluid mechanics and heat transfer data. The great emphasis placed on the development of accurate boundary layer calculation techniques over the past few years reflects the recognition of these needs.

One particularly important topic in the general context of turbine airfoil convective heat transfer is the influence of the free-stream turbulence on both transitional and fully turbulent boundary layer profile development. It has, of course, long been recognized that increasing the free-stream turbulence level can cause a forward shift of the laminar to turbulent transition region. This particular phenomemon, the reduction of the boundary layer transition Reynolds number with increased free-stream turbulence level, is well documented in the open literature for zero pressure gradient flows and can be accurately predicted with at least one currently available boundary layer prediction scheme. The influence of the free-stream turbulence on fully turbulent boundary layers, however, is presently unclear. A number of investigators have studied the effects of free-stream turbulence level on flat wall turbulent boundary layer heat transfer rates and have all reported either negligible or very small effects. In contrast, other experiments which documented the effects of free-stream turbulence on boundary layer growth, profile structure, and skin friction distribution reported very large and important influences. The current contract is being conducted in order to clarify these contradictions.

Both wall heat transfer and detailed boundary layer profile data are being obtained for fully turbulent boundary layers for a range of free-stream turbulence levels to provide data which will definitively indicate the influence that free-stream turbulence level has on fully turbulent boundary layer heat transfer. In addition, these experimental data will be employed to evaluate the turbulence entrainment models currently incorporated in existing boundary layer calculation techniques.

As previously discussed, the effects of free-stream turbulence on the zero pressure gradient boundary layer transition Reynolds number are well understood. The influence of the free-stream turbulence on the transition process becomes considerably less well defined, however, for cases in which the boundary layer is also exposed to a pressure gradient. The net result of the combined influences of turbulence and pressure gradient is dependent upon the sign of the pressure gradient and the relative strengths of the two effects. For adverse pressure gradients both the turbulence and the deceleration promote the transition process and in this case the net result is simply to hasten transition. For favorable pressure gradients, however, the flow acceleration acts to stabilize the boundary layer and tends to counteract the effect of the free-stream turbulence. This interplay of pressure gradient and turbulence results in at least two effects on the transition process; (1) the location of the onset of transition is influenced and (2) the length and character of the transitional boundary layer flow region may be altered significantly. At the present time only very limited experimental data documenting these effects are available. To further complicate the matter, much of the currently available data is contradictory making it impossible to assess the relative quality of boundary layer calculation techniques for these flows. For these reasons, as part of the present contract both wall heat transfer and detailed velocity and temperature profile data will be obtained for accelerating transitional boundary layer flows exposed to high free-stream turbulence levels. These data will be utilized to evaluate the current capability of existing boundary layer calculation procedures to predict boundary layer development with combined favorable pressure gradients and high free-stream turbulence levels.

The present contract program will provide the wall heat transfer and detailed mean boundary layer profile development data required to determine the influence of free-stream turbulence level on both fully turbulent and accelerating transitional boundary layers. These data will be fundamental in nature and could be employed by both UTRC and other workers in the field of boundary layer computation for evaluation of analytical models. In addition the contract experiments will provide a valuable body of detailed heat transfer and boundary layer profile data directly relevant to the problem predicting heat transfer distributions on gas turbine airfoils. Possible requirements for the development of new analytical models for the entrainment of free-stream turbulence into boundary layers and/or new boundary layer transition models will also be established. Finally, as mentioned above, the information could result in more accurate blade heat transfer distribution prediction techniques and thereby the more efficient use of blade cooling air.

The contract effort consist of the documentation and analysis of experimental flat wall boundary layer profile and heat transfer data to determine the influence of free-stream turbulence on transitional and fully turbulent boundary layer flows. For fully turbulent, zero pressure gradient boundary layer flows the following data will be obtained for a range of free-stream turbulence intensities; convective heat transfer coefficients, boundary layer mean velocity and temperature profiles, test wall static pressure distributions, and free-stream turbulence intensity, spectral, and longitudinal integral scale distributions. These same measurements will be obtained for various combinations of favorable pressure gradients and free-stream turbulence levels for transitional boundary layer flows. From these data the integral properties of the test boundary layers will be calculated and, where applicable, the profile data will be reduced to the "universal" coordinates for tubulent boundary layers U^+, Y^+, and T^+. Finally the measured heat transfer distributions and boundary layer profile development will be compared to predictions of the UTRC Finite-Difference Boundary Layer Deck. These comparisons will be employed to evaluate the computation methods currently incorporated in the UTRC deck.

STATUS OF THE RESEARCH EFFORT

During the first year of contract effort convective heat transfer coefficients, boundary layer mean velocity and temperature profiles and wall static pressure distribution data were obtained for two flow conditions of constant free-stream velocity and a free-stream turbulence intensity below 1% and for one flow condition of constant free-stream velocity and free-stream turbulence greater than 1% (a total of 3 flow conditions). These measurements constitute part of Task "a" of the contract Statement of Work. In addition convective heat transfer coefficient and wall static pressure distribution data were obtained for a fourth flow condition of very low tunnel speed (40.3 fps). This low speed test condition was examined as an accuracy check for the heat transfer data reduction system. At least 2 additional flow conditions of constant free-stream velocity and free-stream turbulence greater than 1% will be documented during the second year of the contract effort in fulfillment of Task "a" of the contract Statement of Work.

Description of Test Equipment

UTRC Boundary Layer Wind Tunnel

All experimental data for the present investigation are being obtained in the United Technologies Research Center Boundary Layer Wind Tunnel. This tunnel was designed for conducting fundamental studies of two-dimensional, incompressible flat wall boundary layers flow. Incorporated in the tunnel is a versatile, adjustable test section constructed so that laminar, transitional or turbulent boundary layer can be subjected to favorable, zero, or adverse pressure gradients. In addition, test boundary layers can be subjected to a wide range of free-stream turbulence levels. Low free-stream turbulence flows can be investigated in this facility since it is designed to have a very low residual test section turbulence level. Higher turbulence levels can be generated within the test section through the use of various rectangular grids.

An overall sketch of the Low Speed Boundary Layer tunnel is shown in Fig. 1. The Tunnel is of recirculating design and consists of a blower, a settling chamber/plenum, a contraction nozzle, the boundary layer test section, a downstream diffuser, and a return duct. The settling chamber/plenum consists of a series of perforated part span baffles which even out gross irregularities in the flow from the blower and a honeycomb which removes large scale flow swirl. Downstream of the honeycomb are a series of fine mesh damping screens which progressively reduce both the flow nonuniformity and the residual tunnel turbulence level. A nozzle with a 2.8:1 contraction ratio mounted downstream of the damping screens accelerates the flow to produce the required test section Reynolds numbers. Following the contraction nozzle the flow

passes through the 34 in. wide flat wall boundary layer test section. At the entrance to the test section an upstream facing scoop bleed assembly forms the leading edge of the boundary layer test surface. The purpose of this leading edge bleed scoop is to divert all the flow near the tunnel upper wall. With this arrangement the test section flow consists of the uniform "core" flow from the main contraction nozzle. A sketch showing details of the scoop assembly is presented in Fig. 2. The scoop assembly consists of a two stage leading edge adjustable bleed and, as shown in Fig. 2, is attached to the flat wall boundary layer test surface. The upstream and by far the larger of the two scoops diverts the flow nearest the upper wall of the contraction exit duct. This large scoop is intended to trap both the two-dimensional boundary layer which develops along the contraction nozzle wall and the vortices which develop in the contraction corners. The flow rate along the scoop opening is adjusted by locally restricting portions of the perforated plate located at the scoop exit (see Fig. 2). The local scoop flow rate can be adjusted to produce uniform pressure (in the transverse direction) at the static taps along the entire scoop. The downstream and much smaller of the two scoops is mounted directly on the front edge of the Uniform Heat Flux Flat Wall Model. The test section boundary layer beings growing at the leading edge of this smaller scoop. The purpose of this small-scale second scoop is to provide as short an unheated starting length upstream of the heated test surface as practical by bleeding off any boundary layer which develops along the large scoop lip. As with the larger upstream scoop the flow rate along the small scoop is adjusted by locally restricting portions of the perforated plate located at the small scoop exit (see Fig. 2). The leading edge of the small downstream scoop is a 4 x 1 ellipse shape in order to prevent a local separation bubble and premature transition of the test surface boundary layer. As shown in both Figs. 1 and 2 the flow diverted by the leading edge scoop assembly is returned to the main tunnel loop through a small duct.

The main test section of the Boundary Layer Tunnel consists of the flat upper wall test surface, a lower flexible, adjustable stainless-steel wall and transpartent vertical sidewalls. The vertical sidewalls were constructed of plexiglass to facilitate positioning of boundary layer probes and for purposes of conducting flow visualization studies. Downstream of the test section a diffuser/corner combination reduces the test section velocity and delivers the flow to the return duct. Mounted in this return duct are an air filter and a liquid chilled heat exchanger which controls and stabilizes the tunnel air temperature at approximately 70^{o}F.

A photograph of the Boundary Layer Wind Tunnel is presented in Fig. 3. Also shown in Fig. 3 are both the telescope used to position probes relative to the test wall and the computer controlled probe traverse mechanism.

Uniform Heat Flux Flat Wall Model

As discussed in the Boundary Layer Wind Tunnel description the test boundary layer development begins at the leading edge of the small bleed scoop and continues along the flat test wall. For these present studies the flat wall test surface consists of an electrically heat plate instrumented for the measurement of local convective coefficients. This heated test surface is designed to produce a nearly uniform heat flux distribution over its entire surface and will be referred to as the Uniform Heat Flux Flat Wall Model. This flat wall model consists of a block of rigid urethane foam 34 in. wide by 96 in. long by 4 in. thick mounted in a plexiglass frame with 6 in. wide strips of metal foil cemented to the test surface. A sketch of the Flat Wall Model and its instrumentation is presented in Fig. 4. Rigid foam was employed for the substrate of the Flat Wall Model because of its extremely low thermal conductivity ($k = 0.025$ Btu/hr ft ^{o}F). Because of this low foam conductivity less than 1/2% of the heat generated on the surface of the plate is conducted through the model wall.

Electric current passing through the metal foil strips cemented to the Flat Wall Model test surface produces the surface heating. The metal foil strips are wired in series and are powered by a single low ripple, regulated D.C. power supply. Use of series wiring assures that precisely the same current passes through each of the metal foil surface strips. The metal foil employed for the model surface was 316 stainless, "3/4 hard" temper, 0.0012 in. thick by 6.00 in. wide. The temperature-resistance characteristics of three samples of this foil were determined using an Electro Scientific Industries 1701 B Precision Ohmmeter. A low temperature oven was used to control the temperature of the foil samples. Resistance data obtained for the three samples are presented in Fig. 5. The extremely small scatter for these data indicates that for any test surface temperature the local foil resistance can be calculated within an accuracy of 1% using the following expression.

$$R_{foil} = R_{ref} \left(1 + \alpha_{ref} \left(T_{foil} - T_{ref}\right)\right) \qquad (1)$$

where

$T_{ref} = 71°F$

$R_{ref} = 0.0500\ \Omega/Ft\ @\ 71°F$

$\alpha_{ref}\ @\ 71°F = 0.000504\ \Omega/°F$

The foil test surface is instrumented with an array of 203 Cr-Al 0.005 in. wire diameter bead welded thermcouples. The thermocouple array is shown in Fig. 4. Each thermocouple was welded to the back surface of the foil through a hole in the rigid foam plate. Welding the thermocouple beads directly to the foil insures that the local foil temperatures can be accurately measured.

In order to insure a known, constant test surface emissivity and hence a know radiation loss the completed foil test surface was coated with 3M C-101 high emissivity flat black paint ($\underline{e}$ = 0.99). Forty-eight surface static pressure taps were also installed in the Flat Wall Model. The locations of these static taps are shown in Fig. 4.

Photographs of the Uniform Heat Flux Flat Wall Model at various stages of completion are presented in Figs. 6, 7 and 8. Figure 6 shows the plexiglass frame for the Flat Wall Model prior to casting the rigid urethane foam wall. A photograph of the back surface of the Flat Wall Model is presented in Fig. 7. This photograph shows the leading edge scoop lip mounted on the front edge of the model and the routing of the thermocouple and static pressure leads. Figure 8 shows the test surface of the model before it was coated with high emissivity black paint. In Fig. 8 the surface foil strips have been connected to their respective buss bars. The buss bar/ strip circuit is arranged in series so that the total power current passes through each individual strip.

The D.C. power current passing through the surface strips is measured using two precision shunt resistors and a digital voltmeter. The temperatures of the test surface thermocouples are measured relative to a single test section freestream reference junction using a digital voltmeter.

The local generated power on the test surface is determined by measuring the local wall temperature, Tw, and calculating the local dissipation.

$$q_{power} = I^2 R_{foil} = I^2 R_{ref} (1 + \underline{a}_{ref} (T_w - T_{ref})) \qquad (2)$$

The local convective coefficient can then be determined by ignoring the negligible conduction losses, subtracting that power lost through thermal radiation and dividing by the temperature difference from the wall (T_W) to the freestream (T_e).

$$h = \frac{q_{power} - q_{radiation}}{T_w - T_e} \qquad (3)$$

As an example to illustrate the magnitude of the radiation losses from the test surface, for U_e = 100 fps, for turbulent boundary layer flow with $T_w - T_e = 25^o$ F, the radiation loss is approximately 4 percent of the total surface power. Aside, then, from the small differences in local dissipation and radiation reflected by equations 2 and 3 respectively, the test surface produces uniform convective heat flux for turbulent flow test cases.

Instrumentation

Boundary layer mean velocity profile data will be measured using United Sensor Model BA-0.020 impact probes with flattened tips. A photograph of a typical probe is presented in Fig. 9. The probes to be used in the program were inspected using both a Nikon Model II toolmakers microscope and a Jones and Lamson Model PC14 Shadowgraph. Probe dimensions obtained with these instruments are included in Fig. 9.

Mean temperature data will be measured with miniature thermocouple probes designed using the results of Ref. 1. Photographs of thermocouple probes No. 1 and 2 are presented in Fig. 10. The thermocouple sensing element for these probes is constructed from 0.001 in. dia Chromel-Alumel bead welded wires. The thermocouple bead ($\approx$0.003 in. dia) is located at the center of the probe support prongs which are fabricated of heavier Chromel and Alumel wire. The results of Ref. 1 indicate that a probe of the design will be virtually free of wire conduction errors and is capable of measuring boundary layer mean temperature profile data into the viscous sublayer region.

Data Acquisition System

Experimental data for the UTRC Boundary Layer Wind Tunnel is recorded using a data acquisition system specifically designed for this facility. This data acquisition system is capable of recording time mean analog signals from the various pressure, temperature and hot wire/hot film probes and test section transducers used in the facility. In addition the system controls the movement of the various boundary layer probes through the use of an L.C. Smith ball/screw traverse drive linked to an InterData Model 6/16 computer. Signals from the various probes are recorded using InterData magnetic disks. The data system consists of 2 units (1) a console containing the InterData computer and disk recording unit and a Perkin-Elmer Model 1100 scope/keyboard control terminal and (2) a remote cabinet unit, linked by cables to the console unit, which contains the sensor transducers and traverse controls. The computer cabinet is relatively mobile and can be moved to convenient locations near the tunnel test section. A photograph of Units 1 and 2 of the data acquisition System is presented in Fig. 11. Also, in Fig 3. (tunnel test section photograph) the remote unit can be seen at the downstream end of the test section.

Boundary Layer Analysis

Boundary layer flow has been examined as extensively and throughly as any subject in fluid mechanics. As a result of these investigations, both experimental and analytical, there exists a wealth of information on the topic in the open literature. As the subject area has developed and evolved a number of "standard" or "traditional" methods have arisen for evaluating and examining mean, or time-averaged, profile data. The following section consists of a brief summary of the bases of these "standard" evaluation methods. An explanation of the mean profile data analysis system employed in the present study is also provided. This data analysis system provides an accurate and consistent method of inferring the wall shearing stress from the mean velocity profiles and also, by reducing the profiles to "universal" velocity and temperature coordinates, allows the present results to be compared with other data. Only those aspects of boundary layer flow directly applicable to the present program are discussed within this section (specifically turbulent incompressible, flat wall boundary layer flow). For additional information, generally of a much broader scope, the reader is urged to consult the articles which formed the bases of this summary (Clauser (Ref. 2), Coles (Ref. 3 and 4), Schubauer and Tchen (Ref. 5), Rotta (Ref. 6), Blom (Ref. 7), and Deissler (Ref. 8).

Background

Turbulent boundary layer flows are generally viewed as a composite of four regions, each with its own distinct character. Starting at the wall and moving progressively outward, the first of these four regions consists of an extremely thin layer in which the normal velocity gradients are very large and shearing stresses result only from molecular viscosity ($\tau = \mu \frac{\partial U}{\partial y}$) . This extremely thin region immediately adjacent to the wall is usually referred to as the viscous sublayer. Beyond the viscous sublayer is the second region, usually called the buffer zone, in which turbulent (Reynolds) stresses produced by velocity fluctuations in the flow provide an increasingly important contribution to the effective total shear. The total shear stress relationship is commonly written as:

$$\tau = (\mu + \rho \epsilon_m) \frac{\partial U}{\partial y} \tag{4}$$

where τ is the total shear stress, μ is the molecular viscosity and ϵ_m is the coefficient of eddy diffusivity of momentum.

At the outer edge of the buffer zone the molecular contribution to the total effective shearing stress is negligible. Bradshaw (Ref. 9) presented a comparison of the relative contributions of the molecular and turbulent shearing stresses within the buffer zone. McDonald (Ref. 10) gave a comprehensive analysis of the buffer zone region, including the effects of streamwise pressure gradient. Above the buffer zone in the largest of the three regions yet discussed the molecular shear stresses are negligible and the turbulent stresses dominate the total effective stress. This third region can be described using the so called "law-of-the-wall", to be discussed below. This region will be extensively examined with the present data reduction system and will subsequently be referred to as the "logarithmic law" portion of the boundary layer.

The fourth and last region of the turbulent boundary layer lies between the shear layer (typically 80% of the overall shear layer thickness). Within this "outer" region the mean velocity gradients gradually diminishes until asymptotically approaching zero at the edge of the shear layer. The turbulent shearing stresses also decrease across this outer region but may persist for some small distance beyond the edge of the mean velocity gradient.

Universal Velocity and Temperature Distributions

In the following sections "universal" mean velocity and temperature distributions laws will be presented. As previously discussed these "universal" laws will permit comparison of the present data with that obtained in numerous earlier studies.

Universal Velocity Distribution - Viscous Sublayer and Buffer Zone

In the viscous sublayer turbulent shearing stresses are negligible in Eqn. (4) and:

$$\tau = \mu \frac{\partial U}{\partial y} \qquad (5)$$

Within the sublayer the shear stress is constant and equal to the wall value, τ_w. By integration and rearrangement of Eqn. (5):

$$U = \frac{\tau_w}{\mu} y$$

or in dimensionless form

$$U^+ = y^+$$

where

$$U^+ \equiv \frac{U}{U_\tau} \quad \text{and} \quad y^+ \equiv \frac{yU_\tau}{\nu}$$

$$U_\tau \equiv \sqrt{\tau_w/\rho} \quad = \text{the friction velocity.}$$

It has been experimentally established by numerous investigators that the viscous sublayer extends from the wall to a dimensionless distance of approximately $y^+ = 5$. Figure 12 is a composite velocity distribution for the entire boundary layer and includes the viscous sublayer for $y^+ \leq 5$.

The derivation of velocity distribution laws within the buffer zone is extremely complex and will not be given here. A summary and comparison of many of the buffer zone velocity distribution laws available in the open literature is presented in Ref. 7. For the present program buffer zone velocity data will be compared with the velocity distribution proposed by Burton (Ref. 11). This formulation fulfills all known boundary conditions for the buffer zone, matches all available data well, and blends asymptotically with the well known "law-of-the-wall" (see following section). Burton's proposed buffer zone distribution law is given as follows:

$$y^+ = U^+ + \left(\frac{U^+}{8.74}\right)^7 \tag{6}$$

This distribution law will be employed in the region from $y^+ > 5$ to the outer edge of the buffer zone which is commonly observed to end at approximately $y^+ = 30$ (see Fig. 12).

Universal Velocity Distribution - Logarithmic-Law Region

Prandtl introduced the argument that for a region extending for some unknown distance from the wall the velocity distribution is a function of the wall shear stress, the distance from the wall and the fluid density and viscosity.

$$U = f(\tau_w, y, \mu, \rho)$$

or in dimensionless form

$$\frac{U}{U_\tau} = f_1\left(\frac{U_\tau y}{\nu}\right) \quad \text{where} \quad U_\tau \equiv \sqrt{\tau_w/\rho} \tag{7}$$

For that portion of the shear layer in which the viscous forces are relatively small von Karman suggested the concept of the velocity defect law

He showed that within this region the reduction in velocity below the free-stream value ($U-U_e$) is a function only of the wall shear, the distance from the wall and the overall thickness of the boundary layer

$$U_e - U = f(y, U_\tau, \delta)$$

or in dimensionless form

$$\frac{U_e - U}{U_\tau} = f_2\left(\frac{y}{\delta}\right) \tag{8}$$

Clauser (Ref. 2) has demonstrated the universal validity of Eqn. (8) for constant pressure boundary layers using data obtained for various Reynolds numbers and wall roughnesses.

It has been experimentally demonstrated by numerous investigators that for a significant fraction of the overall shear layer thickness both Eqn. 7 and 8 are valid. Millihan (Ref. 12) was the first to show that if these functions have a region of overlapping validity then the function f_1 and f_2 must be logarithms. This can be seen by writing the functions in the following form

$$\frac{U}{U_\tau} = f_1\left[\left(\frac{y}{\delta}\right)\left(\frac{U_\tau \delta}{\nu}\right)\right] \tag{9}$$

$$\frac{U}{U_\tau} = \frac{U_e}{U_\tau} - f_2\left(\frac{y}{\delta}\right) \tag{10}$$

The function f_1 and f_2 must be logarithms since a comparison of Eqns. (7) and (8) shows that the effect of multiplying factor $\left(\frac{U_\tau \delta}{\nu}\right)$ inside the function of f_1 must be equivalent to the additive term $\frac{U_e}{U_\tau}$ outside the function f_2. This observation has led to the expression commonly referred to as the "law of the wall".

$$\frac{U}{U_\tau} = \frac{1}{\kappa} \ln \frac{y U_\tau}{\nu} + C \tag{11}$$

where κ and C are constants to be experimentally determined.

Taking an alternate approach Prandtl formulated the law-of-the-wall employing the following assumptions. If the turbulent mixing length near the wall is assumed to be proportional to the distance from the wall, $\ell = \kappa y$, and Prandtl's mixing length hypothesis, for the purely turbulent shearing stress, $\tau_t = \rho \ell^2 \left(\frac{\partial U}{\partial y}\right)^2$, is utilized.

then

$$\frac{\tau}{\rho} = \kappa^2 y^2 \left(\frac{\partial U}{\partial y}\right)^2 \qquad (12)$$

(assuming that for this region eddy viscosity >> molecular viscosity then $\tau_t \approx \tau$). Assuming further that shear stress is constant in this region and equal to the wall shear $\tau = \tau_w$ and integrating

$$U = \frac{U_\tau}{\kappa} \ln y + C$$

The constant of integration is determined from the condition that the turbulent velocity distribution must merge with the viscous sublayer velocity distribution near the wall. For details see Schlichting (Ref. 13). Upon rearrangement this yields

$$\frac{U}{U_\tau} = \frac{1}{\kappa} \ln \frac{y U_\tau}{\nu} + C$$

which is identical to Eqn. 11.

It has been experimentally established that the logarithmic "law-of-the-wall" applies, for flows with mild adverse, zero, and mild favorable streamwise pressure gradients, from $30 < \frac{y U_\tau}{\nu} < 100$ to 800 with the upper limit dependent upon the magnitude and sign of the streamwise pressure gradient (see Fig. 12).

Universal Velocity Distribution - Wake Region

As previously discussed, beyond the logarithmic law region of the boundary layer the effects of both molecular and eddy viscosity become decreasingly important. This outermost section of the boundary layer is commonly referred to as the wake region because of its jet-like or wake-like shape (see Coles Ref. 14). Coles (Ref. 4) has extensively examined wake region flow and has developed a comprehensive wall-wake analysis. In Coles' approach, the outer wake region flow is viewed as a deviation from the "law-of-the-wall" and the entire mean velocity profile from $y^+ \cong 30$ to the edge of the shear layer is described by the composite equation

$$\frac{U}{U_\tau} = \frac{1}{\kappa} \ln \frac{y U_\tau}{\nu} + C + \frac{2\Pi}{\kappa} \sin^2\left(\frac{\pi}{2} \frac{y}{\delta}\right) \qquad (13)$$

where the wake strength, Π, is a measure of the maximum deviation of the dimensionless velocity from the law-of-the-wall.

A composite velocity distribution can now be constructed for all four regions of the turbulent boundary layer (see Fig. 12). This universal distribution spans the entire shear layer, from the wall to the free stream.

Universal Temperature Distribution

To this point the development of the universal velocity distribution equations has been concerned with only constant property, isothermal flows. For flows with wall heat transfer a similar set of equations for a universal temperature distribution can be developed and employed for two purposes. First, as with the universal velocity distribution laws, they provide a method for comparing mean temperature profile data from the present program with the data from many other earlier studies. Second, the "temperature-law-of-the-wall" can be employed to infer an average value of the turbulent Prandtl number (P_{r_t}) for the boundary layer.

For turbulent flow the total effective shear and heat flux are the sum of the molecular and turbulent eddy contributions.

$$\tau = (\mu + \rho \epsilon_m) \frac{\partial U}{\partial y}$$

$$q = -\left(k + \rho c_p \epsilon_h\right) \frac{\partial t}{\partial y}$$

where ϵ_m and ϵ_h are the coefficients of eddy diffusivity of momentum and heat respectively.

Written in dimensionless form these equations become

$$\frac{\tau}{\tau_w} = \left(\frac{\mu}{\mu_w} + \frac{\rho \epsilon_m}{\rho_w \mu_w / \rho_w}\right) \frac{\partial U^+}{\partial y^+} \tag{14}$$

and

$$\frac{q}{q_w} = \left(\frac{k}{k_w} \frac{1}{Pr_w} + \frac{\rho}{\rho_w} \frac{c_p}{c_{p_w}} \frac{\epsilon_h}{\mu_w / \rho_w}\right) \frac{\partial t^+}{\partial y^+} \tag{15}$$

where

$$t^+ = \frac{(t_w - t)\,\rho_w c_p \sqrt{\tau_w/\rho}}{q_w} = \frac{t_w - t}{t_\tau}$$

$$t_\tau \equiv \frac{q_w}{\rho_w c_p U_\tau}$$

and $Pr = \frac{\mu c_p}{k}$ = the molecular Prandtl number. For near constant properties (i.e., $k \approx k_w, \rho \approx \rho_w, c_p \approx c_{p_w}$) Eqns. (14) and (15) can be written as

$$\frac{\tau}{\tau_w} = \left(1 + \frac{\epsilon_m}{\nu}\right) \frac{\partial U^+}{\partial y^+} = \frac{\epsilon_{me}}{\nu} \frac{\partial U^+}{\partial y^+} \tag{16}$$

where $\epsilon_{m_e} = \nu + \epsilon_m$ = the effective or total viscosity and

$$\frac{q}{q_w} = \left(\frac{1}{Pr} + \frac{\epsilon_h}{\nu}\right) \frac{\partial t^+}{\partial y^+} = \frac{\epsilon_{h_e}}{\nu} \frac{\partial t^+}{\partial y^+} \tag{17}$$

where $\epsilon_{h_e} = \left(\frac{\nu}{Pr} + \epsilon_h\right)$ = the effective or total thermal diffusivity. If the effective Prandtl number is defined as $Pr_e = \frac{\epsilon_{m_e}}{\epsilon_{h_e}}$ then Eqn. 17 can be written as:

$$\frac{q}{q_w} = \frac{\epsilon_{m_e}}{\nu} \frac{1}{Pr_e} \frac{\partial t^+}{\partial y^+} \tag{18}$$

In Eqn. 18 the heat flux is written in terms of the eddy diffusivity of momentum. Eqn. 13 can be combined with Eqn. 11 to yield

$$\frac{\tau_w q}{\tau q_w} Pr_e \frac{\partial U^+}{\partial y^+} = \frac{\partial t^+}{\partial y^+} \tag{19}$$

If it is assumed that for at least some distance from the wall the shear stress and heat flux are constant and equal to the value near the wall, $\frac{\tau_w q}{\tau q_w} \approx 1$ then Eqn. 19 can then be written as

$$t^+ = \int_0^{U^+} Pr_e \, dU^+ \tag{20}$$

Equation 20 is an important result, indicating that if P_r (U^+) can be obtained then the temperature distribution can be determined. This functional relationship will be developed below. From the definition of the effective Prandtl number and the turbulent Prandtl number ($Pr_t = \frac{\epsilon_m}{\epsilon_h}$)

$$Pr_e = \frac{\epsilon_{m_e}}{\epsilon_{h_e}} = \frac{1 + \frac{\epsilon_m}{\nu}}{\frac{1}{Pr} + \frac{\epsilon_m}{\nu Pr_t}} \tag{21}$$

Using Eqns. (21), (16) and the assumption that $\tau_w \approx \tau$

$$Pr_e = \frac{\left(\frac{\partial U^+}{\partial y^+}\right)^{-1}}{\frac{1}{Pr} + \frac{\left(\left(\frac{\partial U^+}{\partial y^+}\right)^{-1} - 1\right)}{Pr_t}} \tag{22}$$

Thus an approximation to the functional relationship $Pr_e(U^+)$ has been established. Eqn. 22 can now be substituted into Eqn. 20 to yield an expression for the temperature distribution in terms of the molecular and turbulent Prandtl numbers, and the dimensionless velocity and distance from the wall or:

$$t^+ = f\left(Pr, Pr_t, y^+, U^+(y^+)\right)$$

At this point the temperature distribution can be determined for certain portions of the boundary layer. The first solution will be for the temperature distribution in the viscous sublayer ($y^+ < 5$. For this region $U^+ = y^+$ so Eqn. 22 yields $Pr_e = Pr$.

Substituting into Eqn. 20 and integrating:

$$t^+ = \int_0^{u^+} Pr\, du^+$$

$$t^+ = Pr\, u^+ \tag{23}$$

Equation 23 then gives the temperature distribution within the viscous sublayer.

The second region of the boundary layer for which a temperature distribution can be determined is that portion for which the velocity "law-of-the-wall" applies. The "temperature law-of-the-wall" begins at approximately $y^+ = 30$ and extends for some distance dependent upon the particular flow.

The first step required is to integrate Eqn. 20 across the boundary layer to some height Δ

$$t_\Delta^+ = \int_0^{u_\Delta^+} Pr_e\, du^+ = \int_0^{u_\Delta^+} Pr_t\, du^+ + \int_0^{u_\Delta^+} (Pr_e - Pr_t)\, du^+ \tag{24}$$

Equation 24 will be solved by assuming that Pr_t is a constant across the entire boundary layer.

$$t_\Delta^+ = Pr_t \left(u_\Delta^+ + P_s \right)$$

where

$$P_s = \int_0^{u_\Delta^+} \left[\frac{(Pr_e - Pr_t)}{Pr_t} \right] du^+ \tag{25}$$

Equation 21 can be combined with 25 to eliminate Pr_e and yield

$$P_s = \left(\frac{Pr}{Pr_t} - 1 \right) \int_0^{u_\Delta^+} \left(1 + \frac{Pr}{Pr_t} \frac{\epsilon_m}{\nu} \right)^{-1} du^+ \tag{26}$$

In order to evaluate Eqn. (26) for Ps all that is required is a model for the distribution of $\epsilon_m(y^+)/\nu$. Using Eqn. (26) expressions for Ps have been determined for various universal velocity distributions.

A. von Karman (Ref. 15)

$$P_s = 5 \ln\left(1 + 5\frac{Pr}{Pr_t}\right) + 5\frac{Pr}{Pr_t} - 2.5 \ln 30 - 5.5 \qquad (27)$$

B. Spaulding (Ref. 16)

$$P_s = 13.4\left[\left(\frac{Pr}{Pr_t}\right)^{3/4} - 1\right] \qquad (28)$$

C. Jayatilleke (Ref. 17) has compiled an extensive review of proposed distributions of $\epsilon_m(y^+)/\nu$ and ne gives

$$P_s = \frac{A_1}{Pr_t}\left[\left(\frac{Pr}{Pr_t}\right)^{3/4} - 1\right]\left[1 + 0.28 \exp\left(-0.007\frac{Pr}{Pr_t}\right)\right] \qquad (29)$$

with $A_1 = 8.22$ for $Pr_t = 0.9$ and $A_1 = 9.00$ for $Pr_t = 1.00$. Equations 27, 28, and 29 give nearly identical results. For example for $Pr = 0.71$ and $Pr_t = 0.9$ for Eqn. 27 $Ps = -2.07$, for Eqn. 28 $Ps = -2.18$, and for Eqn. 29 $Ps = -1.926$.

With Ps determined the universal temperature distribution in the logarithmic region can be evaluated from Eqns. 11 and 25

$$t^+ = Pr_t\left(\frac{1}{\kappa} \ln y^+ + C + P_s\right) \qquad (30)$$

For a constant turbulent Prandtl number, Pr_t, Eqn. 30 gives the boundary layer temperature distribution from $y^+ \cong 30$ to some value of y^+ dependent on the particular flow. Equation 30 can be employed, then, to infer an average boundary layer turbulent Prandtl number from that portion which has a constant slope when plotted in t^+ vs $\ln y^+$ coordinates.

Property Variations

In the preceding sections only cases with approximately constant fluid properties have been considered. Deissler (Ref. 8), using the von Karman similarity principal and the assumption that the eddy diffusivities of momentum and heat are equal has developed the following variable property expressions for y^+ and t^+.

$$y^+ = \frac{26\, e^{\frac{2\kappa}{\beta}\sqrt{1-\beta(U^+-A+B)}}\left[\frac{2\kappa}{\beta}\sqrt{1-\beta(U^+-A+B)}+1\right]}{e^{-\frac{2\kappa}{\beta}\sqrt{1-B\beta}}\left(\frac{2\kappa}{\beta}\sqrt{1-\beta B}+1\right)} \qquad (31)$$

$$t^+ = U^+ - B + A$$

where $A = U^+$ at $y^+ = 26$
$B = t^+$ at $y^+ = 26$

and $$\beta = \frac{q_w\sqrt{\tau_w/\rho_w}}{c_p\,\tau_w\,t_w}$$

For the profile data to be obtained in the present program $\beta = 0.002$ and Eqn. (31) agrees within 1% with Eqn. (11) for $\kappa = 0.41$ and $C = 5.0$. Because of the near identity between the constant property and variable property solutions to the universal velocity distributions the much simpler constant property approximation will be employed for this program.

Summary

As previously stated, the analytical relationships documented above provide the basis for the boundary layer data reduction system presented in the following paragraphs. Based on these analytical relationships, the data analysis system serves two purposes: (1) it provides an accurate and consistent method for inferring wall-shearing stresses from the mean profile and (2) by reducing the profiles to "universal" velocity and temperature coordinates, it allows the present results to be compared with other data.

Boundary Layer Data Reduction System

A computer program has been written which reduces, plots, and tabulates the velocity and temperature boundary layer profile data obtained by the UTRC Boundary Layer Wind Tunnel Data Acquisition System. Following is a brief description of this reduction program.

a) Mean velocities (U) are measured with miniature flattened Pitot probes. These velocities are corrected for probe Reynolds number and wall blockage effects using the results of Refs. 18, 19 and 20. Except for those measurements extremely close to the wall ($y \sim < 0.010$ in.) the corrections were less than 1% of the measured velocity. The maximum velocity correction (5%) resulted for the case of the probe touching the wall.

b) Friction velocities (U_τ) for each profile are determined by a least squares fit of the velocity profile data from $50 \lesssim y^+ \lesssim 500$ to the "law-of-the-wall" (Eqn. 11)

$$\frac{U}{U_\tau} = \frac{1}{\kappa} \ln \frac{yU_\tau}{\nu} + C \tag{32}$$

where $\kappa = 0.41$

$C = 5.0$

as recommended by Coles (Ref. 3)

Using this value of U_τ the velocity and temperature data are plotted in universal coordinates $U^+ \equiv \frac{U}{U_\tau}$ and $t^+ \equiv \frac{(t_w - t)\rho_w c_p \sqrt{\tau_w/\rho}}{q_w}$ vs $y^+ \equiv \frac{yU_\tau}{\nu}$. The velocity profile data are compared with Eqn. 32 and the temperature data with Eqn. 33.

$$t^+ = Pr_t \left(\frac{1}{\kappa} \ln y^+ + C + P_s \right) \tag{33}$$

where $Pr_t = 0.9$
$\kappa = 0.41$
$C = 5.0$
$P_s = -2.0$

c) The following integral properties are determined

i) displacement thickness $\delta^* = \int_0^\delta \left(1 - \frac{\rho U}{\rho_e U_e}\right) dy$

ii) momentum thickness $\theta = \int_0^\delta \frac{\rho U}{\rho_e U_e} \left(1 - \frac{U}{U_e}\right) dy$

iii) energy-dissipation thickness $\delta^{**} = \int_0^\delta \frac{\rho U}{\rho_e U_e} \left(1 - \frac{U^2}{U_e^2}\right) dy$

iv) enthalpy thickness $\delta_H = \int_0^{\delta_t} \frac{\rho U}{\rho_e U_e} \left(\frac{T - T_e}{T_e}\right) dy$

Measurement of velocity profile data very close ($y^+ \sim < 30$) to a wall is difficult because of the extremely large local velocity gradients and the finite probe tip size. For the velocity profiles measured in this program a flattened impact probe with a probe tip height of approximately 0.007 in (see instrumentation section) is employed. This tip height corresponds to $\Delta y^+ \approx 10$ for most of the profiles (depending on the individual profile U_τ). Because the true distance from the wall to the effective center of the probe tip is uncertain (uncertainty of approximately $\pm$ 0.001 inch) the recommendation of Coles (Ref. 14) has been followed and the integral thicknesses are evaluated using standard sublayer functions very close to the wall. For values of $y^+ < 35$ (approximately 3 probe tip heights) the integral thicknesses are evaluated using the standard velocity sublayer & buffer zone function (Eqn. 6) of Burton (Ref. 11).

$$y^+ = U^+ + \left(\frac{U^+}{8.74}\right)^7$$

The thermocouple boundary layer probes, as described in the instrumentation section, are constructed with 0.001 in dia. sensing elements. Because of this design, accurate temperature data can be obtained very close to the wall (for some profiles even within the viscous sublayer). For this reason it has been possible to use measured temperature data for evaluation of the integral thicknesses from $y^+ = 5$ to the edge of the boundary layer. For $y^+ < 5$ (viscous sublayer) the integral thickness are evaluated using Eqn. 23.

$$t^+ = Pr\, U^+$$

d) The profile "wake strength" (Π) is determined from an iterative solution of two "local friction law" formulations from Coles (Ref. 14)

i) $$\frac{U_e}{U_\tau} = \frac{1}{\kappa} \ell n \frac{\delta U_\tau}{\nu} + C + \frac{2\Pi}{\kappa}$$

ii) $$\left(\frac{\frac{\delta^* U_e}{\nu} - 65}{\frac{\delta U_\tau}{\nu}} \right) = 1 + \Pi$$

Since the term $\left(\frac{U_\tau \delta}{\nu}\right)$ can be eliminated from Eqns. i) and ii) all that is required to solve for Π are values of Ue, U_τ, and δ^*

The wake component

$$W = \frac{\kappa}{\Pi} \left[\frac{U}{U_\tau} - \left(\frac{1}{\kappa} \ell n\, y^+ + C \right) \right] \qquad (34)$$

is plotted vs $\frac{y}{\delta}$ and compared to Coles (Ref. 14) zero pressure gradient wake function

$$W = 2 \sin^2\left(\frac{\pi}{2} \frac{y}{\delta}\right) \tag{35}$$

e) Defect velocities are calculated using the value of U_τ determined in b

$$\text{Velocity Defect} = \frac{U-U_e}{U_\tau}$$

The defect velocity distribution is plotted vs $\frac{y}{\delta}$ and compared with inner and outer region defect correlations

i) In the inner region ($\frac{y}{\delta} < 0.2$) with the correlation to Schubauer and Tchen (Ref. 5)

$$\frac{U-U_e}{U_\tau} = \frac{1}{\kappa} \ell n\left(\frac{y}{\delta}\right) - 2.35 \tag{36}$$

ii) in the outer region ($\frac{y}{\delta} > 0.2$) with the correlation of Hama (Ref. 21)

$$\frac{U-U_e}{U_\tau} = -9.6 \left(1 - \frac{y}{\delta}\right)^2 \tag{37}$$

f) the following is a list of all plots constructed, including those discussed in parts b, d, and e

i) $\frac{U}{U_e}$ vs $\frac{y}{\delta}$

ii) $\frac{T_w-T}{T_w-T_e}$ vs $\frac{y}{\delta}$

iii) U^+ vs Y^+ (see b)

iv) T^+ vs Y^+ (see b)

v) $\frac{U-U_e}{U_\tau}$ vs $\frac{Y}{\delta}$ (see d)

vi) W vs $\frac{y}{\delta}$ (see e)

g) The following boundary layer values are tabulated

$$y,\ \frac{y}{\delta},\ U,\ T,\ \frac{U}{U_e},\ \frac{T_w - T}{T_w - T_e},\ \frac{U - U_e}{U_\tau},\ U^+,\ Y^+,\ T^+$$

Sample Reduced Boundary Layer Profile Data

The following mean velocity and temperature boundary layer profile data were obtained in the UTRC Boundary Layer Wind Tunnel with the test section adjusted for zero pressure gradient flow. Following are lists of the profile test conditions and measured properties. The plotted results and tabulated data are presented in Figs. 13A, 13B, and 14.

Test Conditions

distance from leading edge - 36.4 in.
free stream density - 0.0720 lbm/ft^3
free stream temperature - 85.0° F
wall temperature - 106.7° F
free stream velocity - 101.1 fps
convective wall heat flux - 0.0749 Btu/sec-ft^2
unheated length upstream of heat flux - 1.7 in.
boundary layer trip location - 1.5 in.

Measured and Calculated Boundary Layer Values

Re_x	-	1.791×10^6
θ	-	0.0689 in.
δ^*	-	0.0997 in.
δ^{**}	-	0.1213 in.
δ_h	-	0.00271 in.
Re_θ	-	3389
Re_{δ^*}	-	4901
δ^*/δ	-	1.446
δ^{**}/δ^*	-	1.760
C_f	-	0.003080
Π	-	0.559

Results To Date

During the first year of contract effort convective heat transfer coefficient data, boundary layer mean velocity and temperature profile data, and wall static pressure distribution data were obtained for two flow conditions of constant free-stream velocity (nominally 100 f/s) and a free-stream turbulence intensity below 1 percent and for one flow condition of constant free-stream velocity (nominally 100 fps) and free-stream turbulence intensity greater than 1 percent (a total of 3 flow conditions). In addition, convective heat transfer coefficient data were obtained for a fourth flow condition of very low tunnel speed (nominally 40 f/s) as an accuracy check for the heat transfer data reduction system.

Stanton number distributions measured for constant nominal free-stream velocities of 40 and 100 fps are presented in Fig. 15. Examination of Fig. 15 reveals that for the nominally 100 fps test case the measured heat transfer distribution, upstream of boundary layer transition ($Re_x < 1.2 \times 10^6$, $x <$ 23 in.), agrees very well with the analytical solution of Ref. 22 (Equation 38 below) for zero pressure gradient, laminar boundary layer flow with a uniform convective heat flux wall and an unheated starting length ξ. For this test plate $\xi = 1.69$ in.

$$St\ Pr^{2/3} = 0.453\ Re_x^{-1/2}\ \left[1 - (\xi/x)^{3/4}\right]^{-1/3} \qquad (38)$$

For the 40 fps test case the measured heat transfer distribution agreed with Eqn. 38 within approximately 5 percent from the beginning of wall heating ($x = \xi = 1.69$ in) to $Re_x \approx 5 \times 10^5$ ($x = 25$ in.). Between $Re_x \approx 5 \times 10^5$ and $Re_x \approx 1.1 \times 10^6$ (where the test boundary layer underwent transition), the measured heat transfer was up to 10 percent less than was calculated by the uniform heat flux prediction of Equation 38. This deviation from Equation 38 is a result of significant surface radiation heat losses present for the 40 fps test case. Unlike the example of high speed turbulent boundary layer flow cited earlier, for the case of low speed laminar boundary layer flow the convective coefficient drops to extremely low values and surface radiation losses become large. For the 40 fps test case at $Re_x = 1 \times 10^6$ nearly 50 percent of the power being generated on the test surface was lost through thermal radiation. Because of these relatively large test wall radiation losses in the 40 fps test case, the convective heat flux progressively and significantly decreases with increasing x. As a result of these radiation losses, the uniform convective heat flux solution (Eqn. 38) is inappropriate for the 40 fps test case. A prediction of the Stanton number distribution for the 40 fps test case was computed using the UTRC Finite-Difference Boundary

Layer Computation code. The code was used to predict a laminar boundary layer flow with the convective wall heat flux distribution present for the actual experimental test case. A comparison of this prediction, also shown in Fig. 15, and the measured distribution shows excellent agreement.

Downstream of $Re_x \approx 1.2 \times 10^6$ the test wall boundary layers passed through transition for both the 40 and 100 fps cases. From $Re_x \approx 1.8 \times 10^6$ to the downstream end of the plate the measured heat transfer data agreed within approximately ± 3 percent with the fully turbulent correlation of Ref. 22.

$$St\ Pr^{0.4} = 0.0307\ Re_x^{-0.2}\ (Tw/Te)^{-0.4} \qquad (39)$$

The conclusion reached from Fig. 15 is that there is excellent agreement, even at very low freestream velocities, between low freestream turbulent heat transfer data measured in this facility and the appropriate analytical predictions or established data correlations.

During the first year of contract effort boundary layer mean velocity and temperature profile data were obtained for three test cases. For all three test cases there was a constant free-stream velocity of nominally 100 fps. The various flow conditions are as follows.

(1) low free-stream turbulence (<1/2 percent) and natural transition of the test wall boundary layer.

(2) low free-stream turbulence (<1/2 percent) and forced (artificially tripped) transition of the test wall boundary layer.

(3) natural transition of the test wall boundary layer and a relatively coarse turbulence generating grid (designated Grid No. 3) installed in the wind tunnel.

Freestream turbulence intensity, spectral, and longitudinal integral scale distributions in the flow downstream of Grid No. 3 are currently being obtained.

Flow Condition 1 - Low Free-stream Turbulence, Natural Transition

The data obtained for flow condition 1 can be compared directly to correlations available in the open literature. In Fig. 16a the measured Stanton number distribution data, which were previously presented as part of Fig. 15

are compared with well established laminar and fully turbulent correlations. Upstream of boundary layer transition ($Re_x < 1.2 \times 10^6$ x < 23 in.), these data agree very well with the analytical solution of Ref. 22 for zero pressure gradient, laminar boundary layer flow with a uniform convective heat flux wall and an unheated starting length. Downstream of $Re_x \gtrsim 1.2 \times 10^6$ the boundary layer passed through transition. From $Re_x \gtrsim 1.8 \times 10^6$ to the downstream end of the plate the measured heat transfer data agreed within $\pm$ 2 percent with the fully turbulent correlation of Ref. 22. In Fig. 16b skin friction coefficient measurements inferred from the mean velocity profile data are compared to the well known incompressible turbulent boundary layer skin friction law formulations of Coles (Ref. 3) and Rotta (Ref. 6). These correlations, which apply for isothermal incompressible turbulent boundary layer flow have been corrected for density variations due to wall heating using Coles' "law of corresponding stations" (Ref. 3). As can be seen from Fig. 16b the measured skin friction coefficients are bracketed by the two correlations.

Fig. 17a presents accuracy and consistency checks calculated for the measured profile data. The momentum balance of Fig. 17a consists of a ratio of the experimentally measured terms of the two-dimensional von Karman Momentum Integral equation. Coles (Ref. 3), in a comprehensive turbulent boundary layer survey article, selected 10 studies as having produced the "best" available two dimensional profile results. A direct comparison can be made between the momentum balance results of Fig. 17a and the results from these "best available" profiles presented by Coles in Fig. 12 of Appendix A in Ref. 3. For the comparable Reynolds number range the present results deviate from an exact momentum balance approximately one-half as much as these "best" selected data. This favorable comparison indicates a high degree of flow two-dimensionality for the present experimental apparatus.

The thermal energy balance data of Fig. 17a is a ratio of the total convective heat generated per unit tunnel width upstream of any profile location to the measured thermal energy contained in the boundary layer at the location. Fig. 17a reveals that this thermal energy balance is also within approximately 5 percent of unity for all the measured profiles. The conclusion reached from Fig. 17a is that the profile data forms an accurate, consistant set and that the flow is highly two-dimensional.

The measured momentum and displacement thicknesses for the various boundary layer profiles are presented in Fig. 17b. As can be seen from an examination of this figure, there is negligible variation between profiles measured at various transverse but fixed streamwise locations on the test surface. In addition, mean velocity and temperature profiles measured at three transvere locations in the laminar flow upstream of boundary layer transition are presented in Fig. 18. The profiles of Fig. 18 were obtained on the tunnel centerline and at stations 6 in to the east and west of the tunnel centerline at x = 12 in, $Re_x = 0.63 \times 10^6$. The measured velocity and temperature profile data

agree extremely well with the laminar boundary layer profile solutions of Blasius (velocity, Ref. 13) and Levy (temperature, Ref. 23) and show negligible transverse variations. Finally, the transverse and streamwise pressure distributions on the test surface leading edge scoop and on the test surface itself are presented in Figs. 19 and 20 respectively. Figs. 19 and 20 indicate that both transverse and streamwise pressure gradients were negligible. The conclusion reached for Figs. 16 through 20 is that the data obtained for this low free-stream turbulence, natural transition case are in excellent agreement with classic two-dimensional correlations.

Flow Condition 2 - Low Free-stream Turbulence, Forced Transition

The profile and heat transfer data obtained for flow condition 2 are presented in Figs. 21 through 24. For the forced transition case, a "triangular patch" boundary layer tripping device as suggested by Hama (Ref. 24) was employed. The advantage of this type of tripping device is that it closely simulates the natural transition process, producing very small scale three-dimensional vortices within the laminar boundary layer. For this test the trip was located at x = 1.5 in. The thickness of the tape used for the triangular patches was 0.007 in. Fig. 21a indicates that from the beginning of plate heating to $Re_x \lesssim 0.8 \times 10^6$ (near the boundary layer trip) the measured Stanton numbers are in excess of those predicted by the correlation of Ref. 22 From $Re_x \lesssim 0.8 \times 10^6$ to the downstream end of the plate, the agreement between the measured data and the correlation of Ref. 22 is excellent, typically with ± 2 percent. As with the low free-stream turbulence, natural transition data of Fig. 16b the data of Fig.21b are bracketed by the well established correlations of Coles and Rotta. Figs. 22a and b indicate that the test boundary layer satisfied the momentum and energy balances within ± 4 percent and was highly two-dimensional. Figs. 23 and 24 indicate that the transverse and streamwise pressure gradients across the leading edge scoops and along the test wall were negligible. The skin friction coefficients and Stanton numbers measured in the equilibrium region far from the boundary layer trip agree very well with those measured downstream of natural transition for flow condition 1. The data obtained for flow conditions 1 and 2, then are consistent with each other and also with well established classic results. These low free-stream turbulence skin friction and heat transfer data will provide a basis of comparison for the rest of the data which will be obtained with higher free-stream turbulence levels.

Flow Condition 3 - Natural Transition, Turbulence Grid No. 3

The profile and heat transfer data obtained for flow condition 3 are presented in Figs. 25 through 28. An examination of Fig. 25a reveals that Stanton numbers measured with this free-stream turbulence distribution were

typically 12 percent in excess of the low free-stream turbulence correlation of Ref. 22. Fig. 25b reveals a similar 12 percent increase in measured skin friction coefficients above the classic skin friction laws for low free-stream turbulence. This result of increased skin friction with increasing free-stream turbulence is in agreement with the experimental results of Refs. 25 and 26 which were obtained for incompressible, unheated flows. Figs. 26a and b indicate that for flow condition 3 the test boundary layer was two-dimensional while Figs. 27 and 28 indicate that the transverse and streamwise pressure gradients along the leading edge scoops and test wall were neglibible. The data obtained for flow condition 3 indicates that free-stream turbulence does have a very significant effect on fully turbulent boundary layer heat transfer. A quantitative assessment of the magnitude of this influence will emerge as data is obtained for additional turbulence grids and as the turbulence distributions generated by these grids are documented.

LIST OF SYMBOLS

C_f - skin friction coefficient, $\frac{2\tau_w}{\rho U_e^2}$

c_p - specific heat at constant pressure

I - strip current

k - thermal conductivity

ℓ - mixing length

Pr - molecular Prandtl number,

Pr_t - turbulent Prandtl number, $\frac{\epsilon_m}{\epsilon_h}$

P_{r_e} - effective Prandtl number, $\frac{\epsilon_{m_e}}{\epsilon_{h_e}} = \frac{1 + \frac{\epsilon_m}{\nu}}{\frac{1}{Pr} + \frac{\epsilon_m}{\nu Pr_t}}$

q - heat flux

R_{foil} - unit resistance of heater foil

Re_x - Reynolds number based on distance from leading edge

Re_θ - Reynolds number based on boundary layer momentum thickness

St - Stanton number, $\frac{h}{\rho U c_p}$

t - temperature

t^+ - dimensionless temperature, $\frac{(t_w - t)\rho_w c_p \sqrt{\tau_w/\rho}}{q_w}$

U - velocity

U^+ - dimensionless velocity, $\frac{U}{U_\tau}$

U_τ - friction velocity

W - wake function, $\frac{U^+ - \frac{1}{\kappa} \ln Y^+ + C}{\Pi}$

x - distance from leading edge

y - distance from wall

Y^+ - dimensionless distance from wall, $\frac{y U_\tau}{\nu}$

LIST OF SYMBOLS (Cont'd)

α - temperature coefficient of resistance

δ - boundary layer thickness

δ^* - displacment thickness, $\int_0^{\delta}\left(1-\frac{\rho U}{\rho_e U_e}\right) dy$

δ^{**} - energy dissipation thickness, $\int_0^{\delta} \frac{\rho U}{\rho_e U_e}\left(1-\frac{U^2}{U_e^2}\right) dy$

δ_H - enthalphy thickness, $\int_0^{\delta_1} \frac{\rho U}{\rho_e U_e}\left(\frac{T-T_e}{T_e}\right) dy$

ϵ - surface emissivity

ϵ_h - coefficient of eddy diffusivity of heat

ϵ_{h_e} - coefficient of effective thermal diffusivity

ϵ_m - coefficient of eddy diffusivity of momentum

ϵ_{m_e} - coefficient of effective viscosity

θ - momentum thickness, $\int_0^{\delta} \frac{\rho U}{\rho_e U_e}\left(1-\frac{U}{U_e}\right) dy$

κ - von Karman constant

μ - molecular viscosity

ν - kinematic viscosity

ξ - unheated starting length

π - wake strength

ρ - fluid density

τ - shearing stress

τ_t - turbulent shearing stress

LIST OF SYMBOLS (Cont'd)

Subscripts

e - freestream

w - wall

REFERENCES

1. Blackwell, B. F. and R. J. Moffat: Design and Conduction of a Low Velocity Boundary-Layer Temperature Probe, AIAA Paper No. 74-709, ASME Paper No. 74-HT-29, July 1974.

2. Clauser, F. H.: The Turbulent Boundary Layer, Advances in Applied Mechanics, Vol. IV, 1956.

3. Coles, D. E.: The Turbulent Boundary Layer in a Compressible Fluid, Rand Report, R-403-PR, 1962.

4. Coles, D. E.: The Law of the Wake in the Turbulent Boundary Layer, JFM, Vol. 1, 1956.

5. Schubauer, G. B. and Tchen, C. M.: "Turbulent Flow" in Turbulent Flows and Heat Transfer, High Speed Aerodynamics and Jet Propulsion, Vol. 5, Princeton University Press, Princeton, N. J., 1959.

6. Rotta, J. C.: Turbulent Boundary Layers in Incompressible Flow, Progress in Aeronautical Sciences, Vol. 2, Pergamon Press Ltd., London, 1962.

7. Blom, J.: An Experimental Determination of the Turbulent Prandtl Number in a Developing Temperature Boundary Layer, Ph.D. Thesis, Technological University, Eindhoven, The Netherlands, 1970.

8. Deissler, R. G.: Heat Transfer and Fluid Friction for Fully Developed Turbulent Flow of Air and Supercritical Water With Variable Fluid Properties, Trans. ASME 76, 1954.

9. Bradshaw, P.: An Introduction to Turbulence and Its Measurement, Pergamon Press Ltd., Oxford, 1971.

10. McDonald, H.: The Effect of Pressure Gradient in the Law of the Wall in Turbulent Flow, JFM, 35, 1969.

11. Burton, R. A.: A Simple Universal Velocity Profile Equation, AIAA Journal 3, 1965.

12. Millikan, C. G.: A Critical Discussion of the Turbulent Flows in Channels and Circular Tubes, Proc. Fifth Intern. Congress Appl. Mech., Cambridge, MA, 1938.

13. Schlicting, H.: Boundary Layer Theory, 6th Edition, McGraw-Hill Book Company, New York, pp 125-133 and 544-556, 1968.

REFERENCES (Cont'd)

14. Coles, D.: Proceedings, Computations of Turbulent Boundary Layers - 1968, AFOSR-IFP, Stanford Conference, Vol. II, 1968.

15. von Karman, T.: The Analogy Between Fluid Friction and Heat Transfer, Trans ASME 61, 1939.

16. Spaulding, D. B.: A Single Formula for the Law of the Wall, J. Appl. Mech., 28, 1961.

17. Jayatilleke, C. L. V.: The Influence of Prandtl Number and Surface Roughness on the Resistance of the Laminar Sublayer to Momentum and Heat Transfer, Progress in Heat and Mass Transfer, Vol. 1, Pergamon Press Ltd., London, 1969.

18. MacMillan, F. A.: Viscous Effects in Flattened Pitot Tubes at Low Speeds, Journal of Royal Aeronautical Society, Vol. 58, 1954.

19. Quarmby, A. and H. K. Das.: Displacement Effects on Pitot Tubes With Rectangular Mouths, The Aeronautical Quarterly, May 1969.

20. MacMillan, F. A.: Experiments in Pitot Tubes in Shear Flow, A.R.C. R&M 3028, 1957.

21. Hama, F. R.: Boundary-Layer Charcteristics for Smooth and Rough Surfaces, Trans. Soc. Naval Architects Marine Engrs. 62, 1954.

22. Kays, W. M.: Convective Heat and Mass Transfer. McGraw-Hill Book Company, N. Y., pp. 222 and 244, 1966.

23. Levy, S.: Heat Transfer to Constant-Property Laminar Boundary-Layer Flows with Power-Function Free-Stream Velocity and Wall-Temperature Variation, J. aeronautical Sciences, Vol. 19, pp. 341, 1952.

24. Hama, F. R.: An Efficient Tripping Device. Journal Aeronautical Sciences, Vol. 24, March 1957.

25. Huffman, G. D., Zimmerman, D. R. and Bennet, W. A.: The Effect of Freestream Turbulence Level in Turbulent Boundary Layer Behavior. AGARD AG164, pp. 91-115, 1972.

26. Charnay, G., Compte-Bellot, G. and Mathiew, J.: Development of a Turbulent Boundary Layer on a Flat Plate in an External Turbulent Flow, AGARD, CP 93, Paper No. 27, 1971.

REFERENCES (Cont'd)

27. Scharnhorst, R. K., Walker, J. D. A. and Abbott, D. E.: Comparison of Theoretical Profiles for a Two-Dimensional Time-Mean Turbulent Boundary Layer with Experimental Data, Purdue Univ. Tech Report CFMTR-77-1, June 77, also AFOSR TR-77-0877.

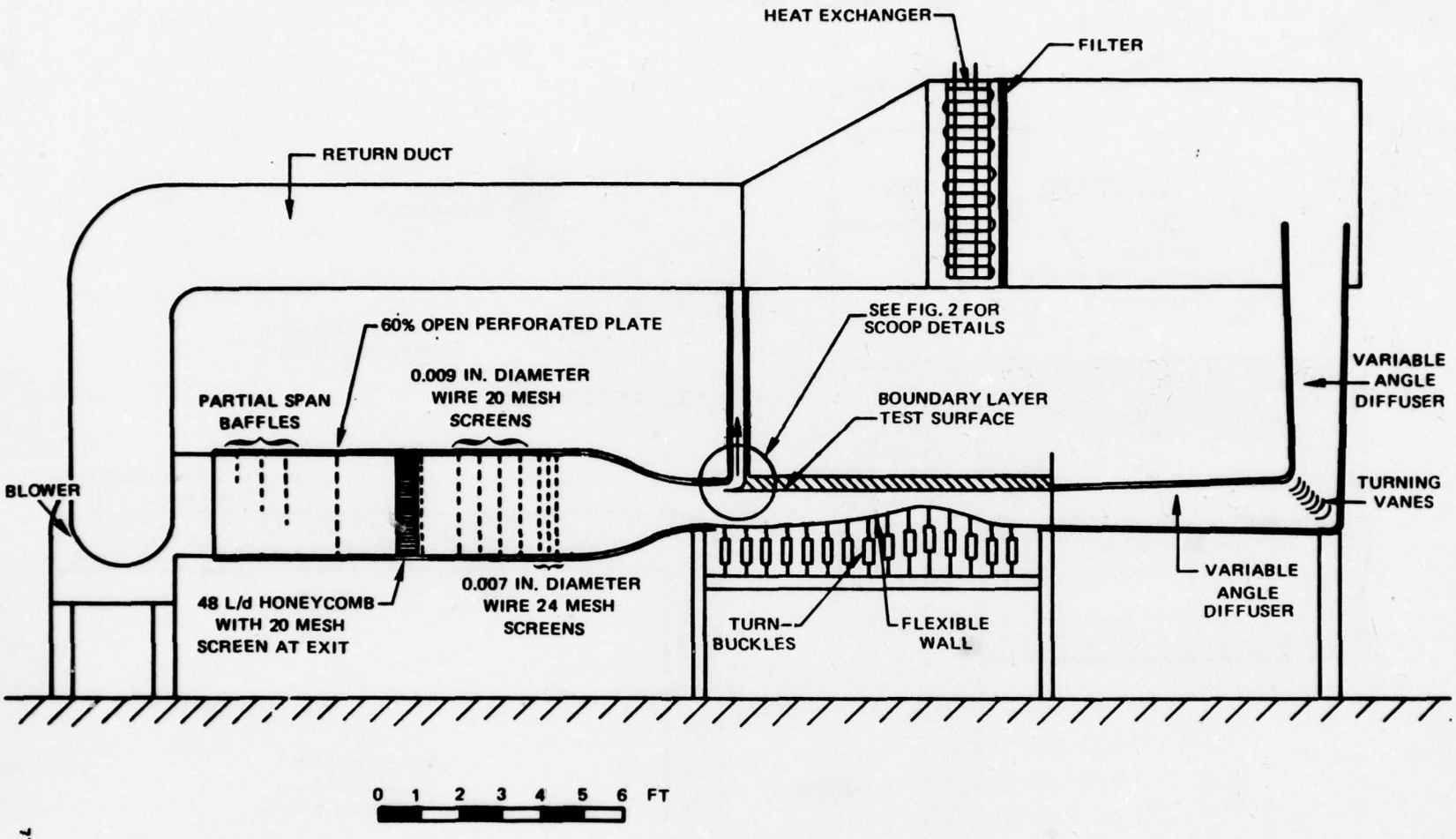

77-06-26-1

Figure 1. United Technologies Research Center Boundary Layer Wind Tunnel

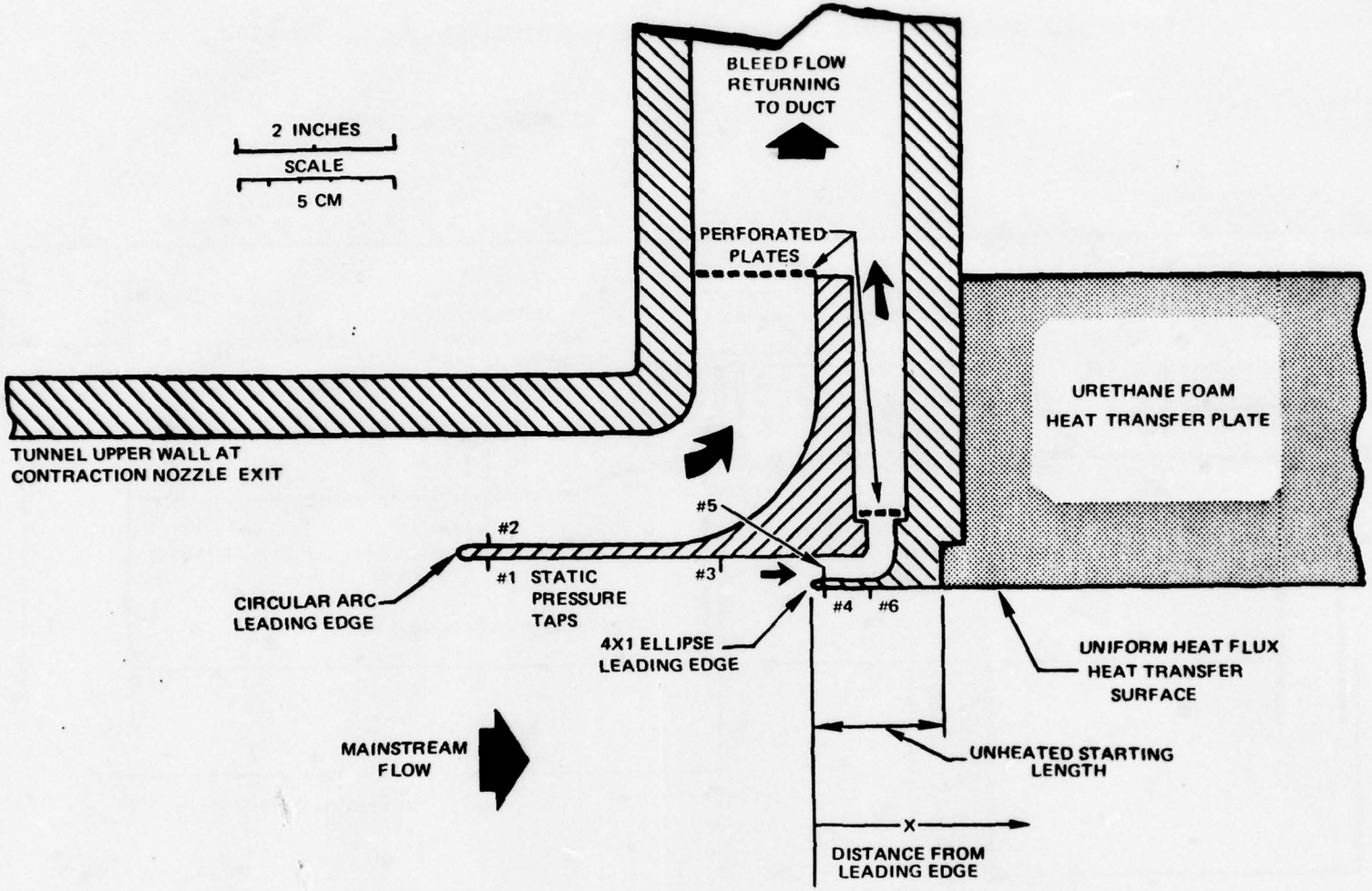

Figure 2. Detailed Sketch of Test Wall Leading Edge Bleed Scoop

78-09-102-1

78-322-D

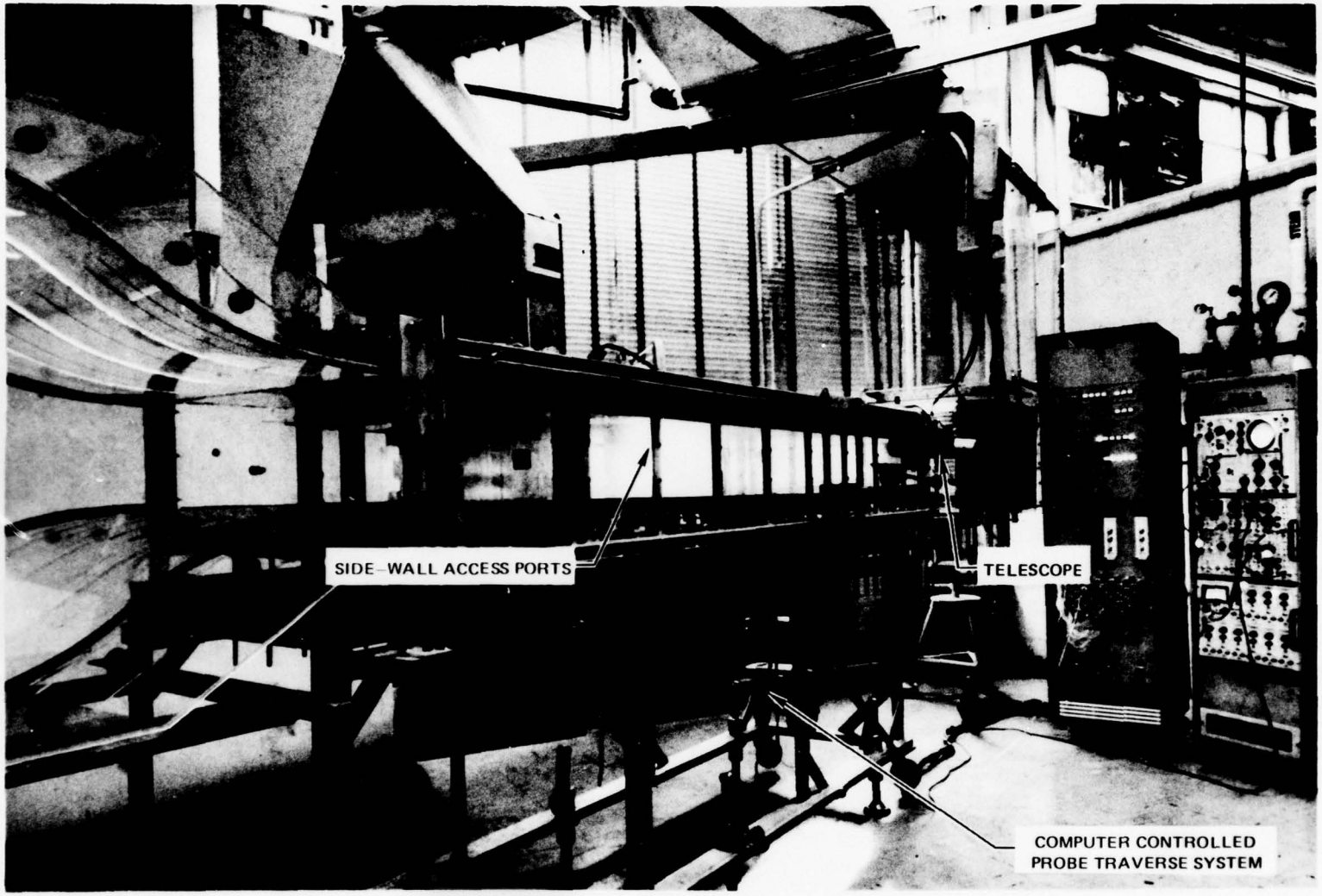

Figure 3. Photograph of UTRC Boundary Layer Wind Tunnel Test Section

78-10-125-9

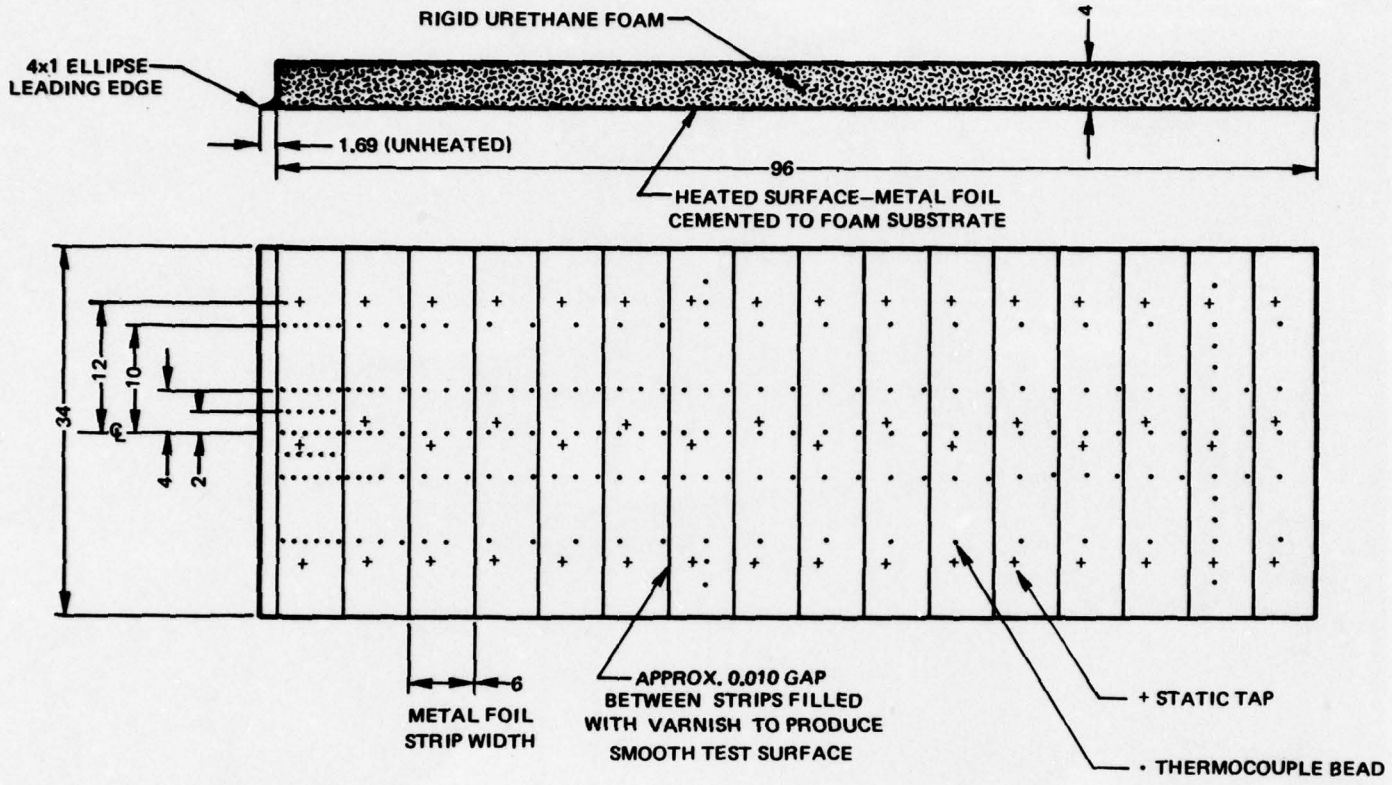

Figure 4. Instrumentation Diagram for the Uniform Heat Flux Flat Wall Model

79-05-70-4

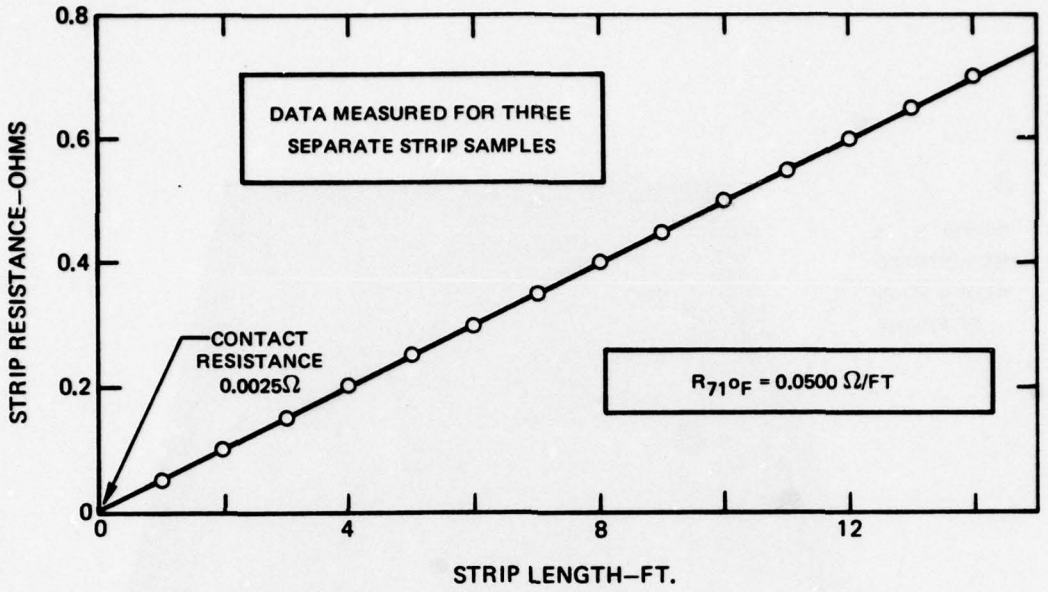

a. 316 STAINLESS STEEL FOIL RESISTANCE AT 71°F

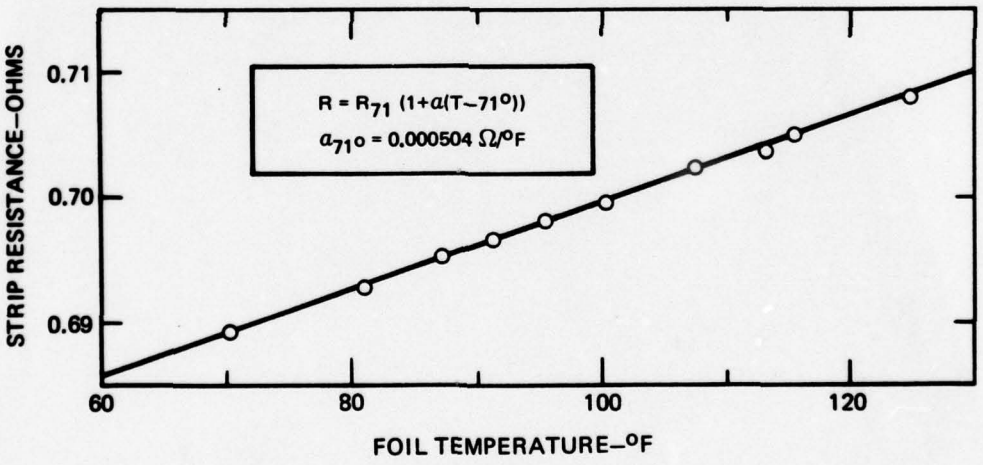

b. 316 STAINLESS STEEL FOIL TEMPERATURE RESISTANCE COEFFICIENT

Figure 5. Electrical Resistance Characteristics of the 316 Stainless Steel Foil Strip Used for the Heated Test Surface of the Uniform Heat Flux Flat Wall Model

79-05-70-5

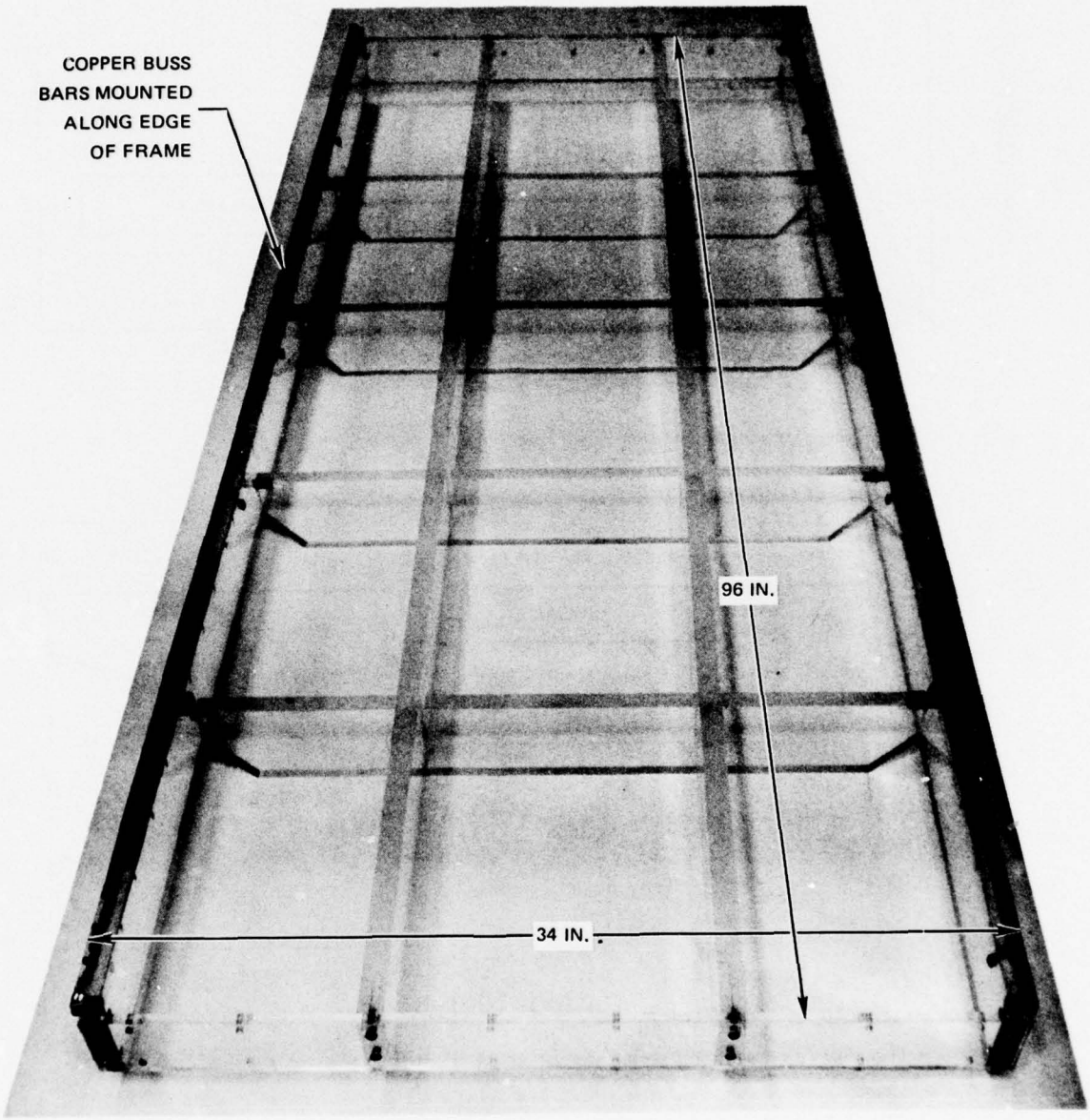

Figure 6. Photograph of the Assembled Plexiglas Frame for the Uniform Heat Flux Flat Wall Model with the Buss Bars Installed

79-05-70-1

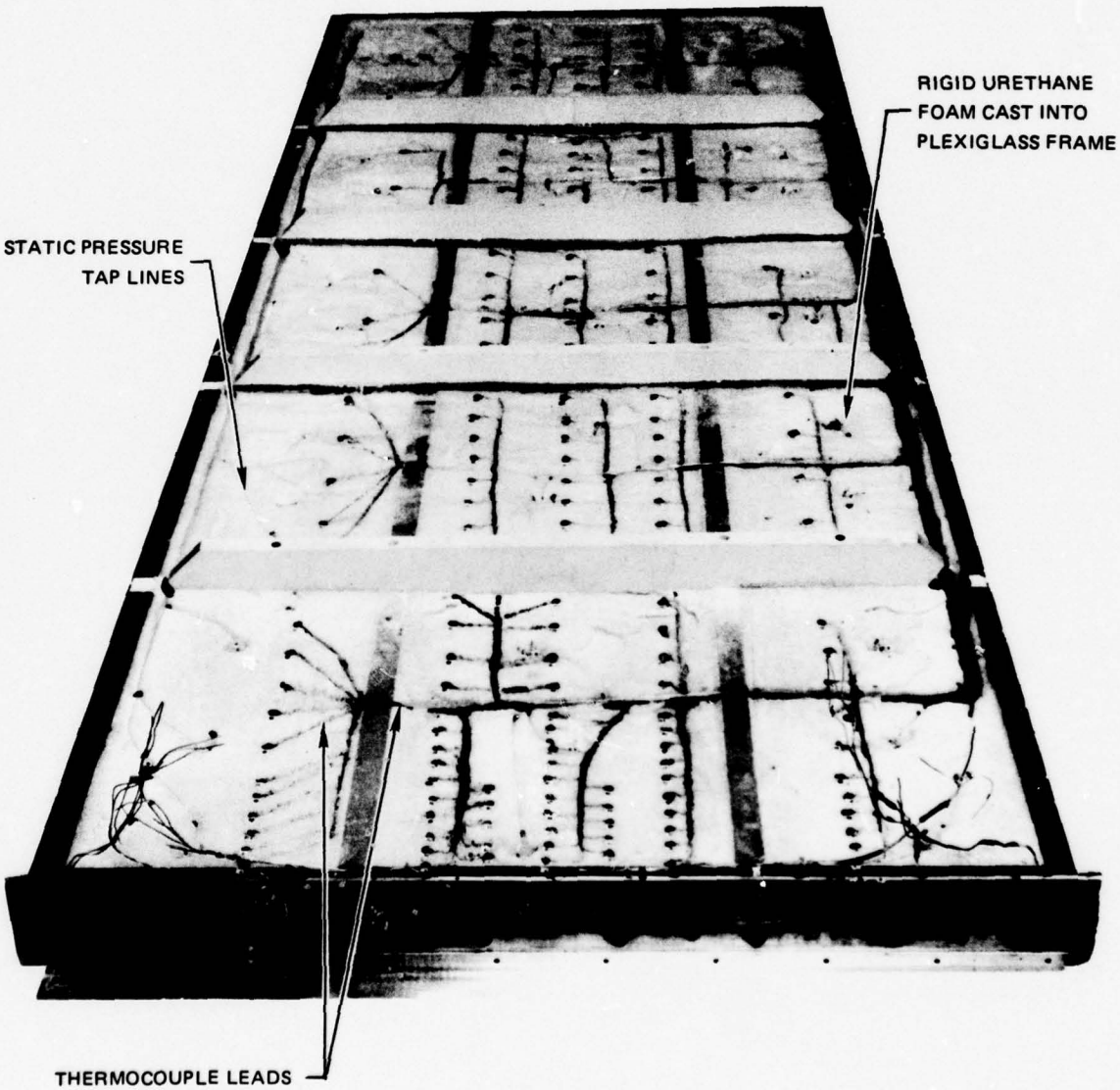

Figure 7. Photograph of the Backside of the Completely Assembled and Instrumented Uniform Heat Flux Flat Wall Model Showing the Routing of the Instrumentation Leads

79-05-70-2

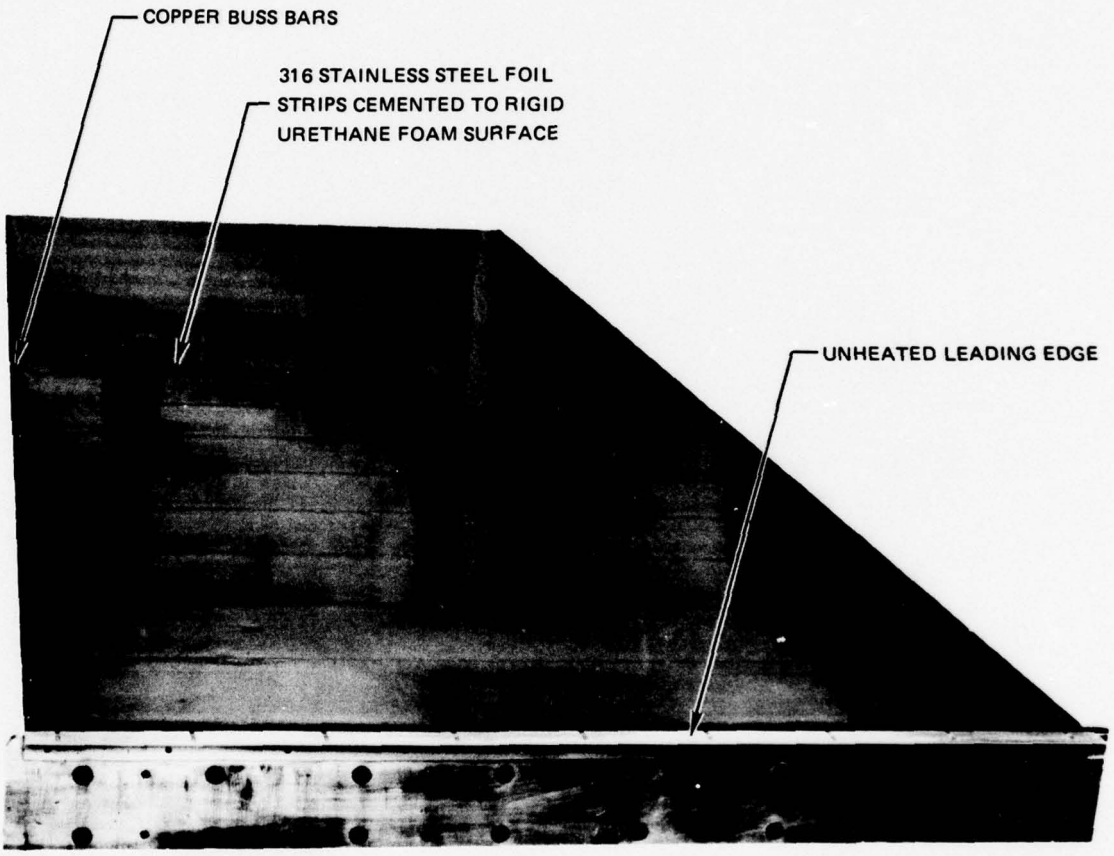

Figure 8. Photograph of Test Surface of the Uniform Heat Flux Flat Wall Model Prior to Coating with High Emissivity Paint

79-05-70-3

78-294-A

a) PROBE TIP DIMENSIONS MEASURED WITH NIKON MODEL II TOOLMAKERS MICROSCOPE

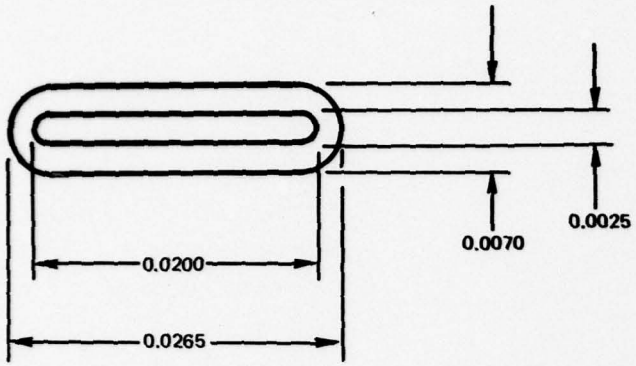

b) SIDE VIEW PHOTOGRAPH OF PROBE

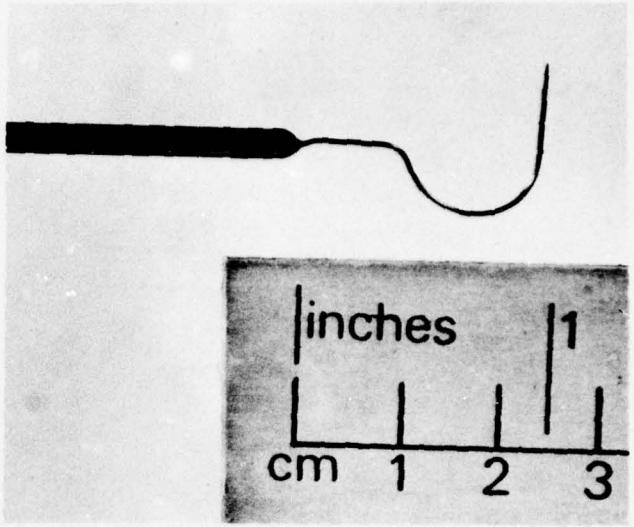

c) MAGNIFIED VIEWS OF PROBE TIP USING JONES AND LAMSON MODEL PC 14 SHADOWGRAPH

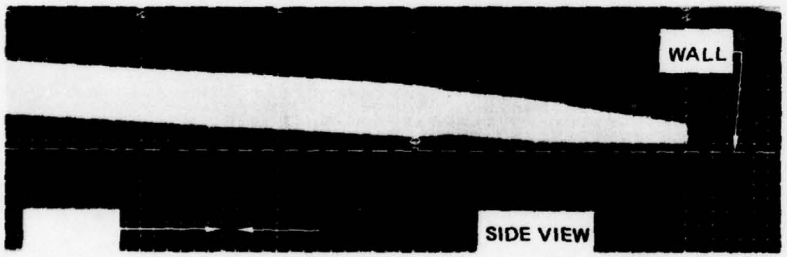

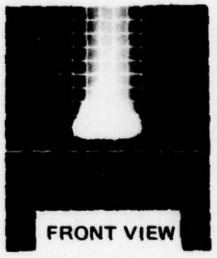

Figure 9. Typical Boundary Layer Pitot Probe Details

78-09-157-1

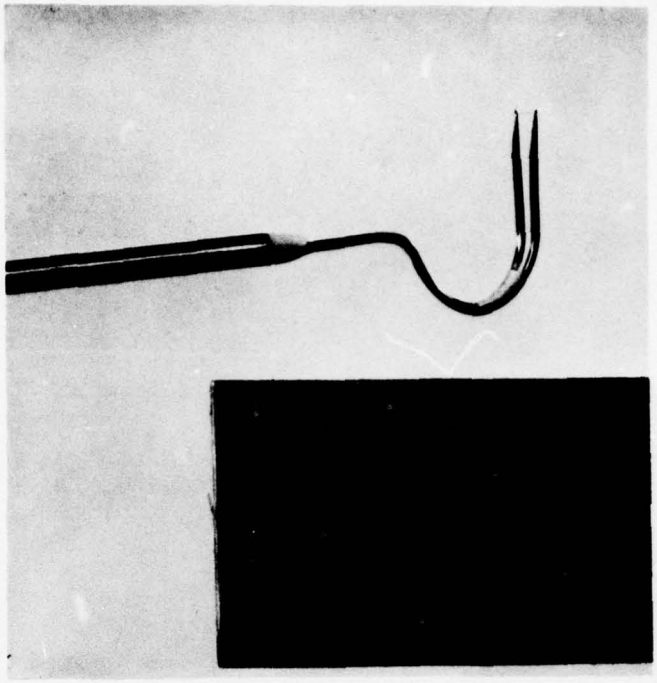

a) TEMPERATURE PROBE NO. 1

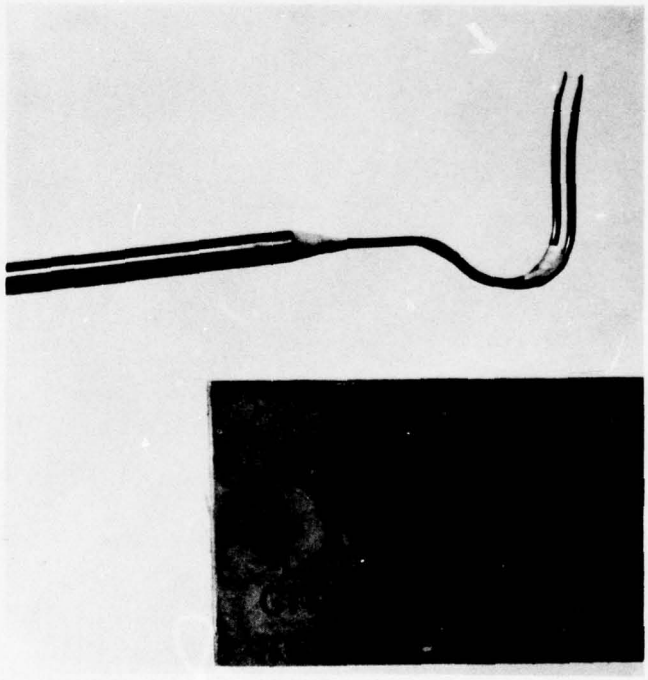

b) TEMPERATURE PROBE NO. 2

Figure 10. Typical Boundary Layer Thermocouple Probes

78-294-D
78-294-E

78-09-157-3

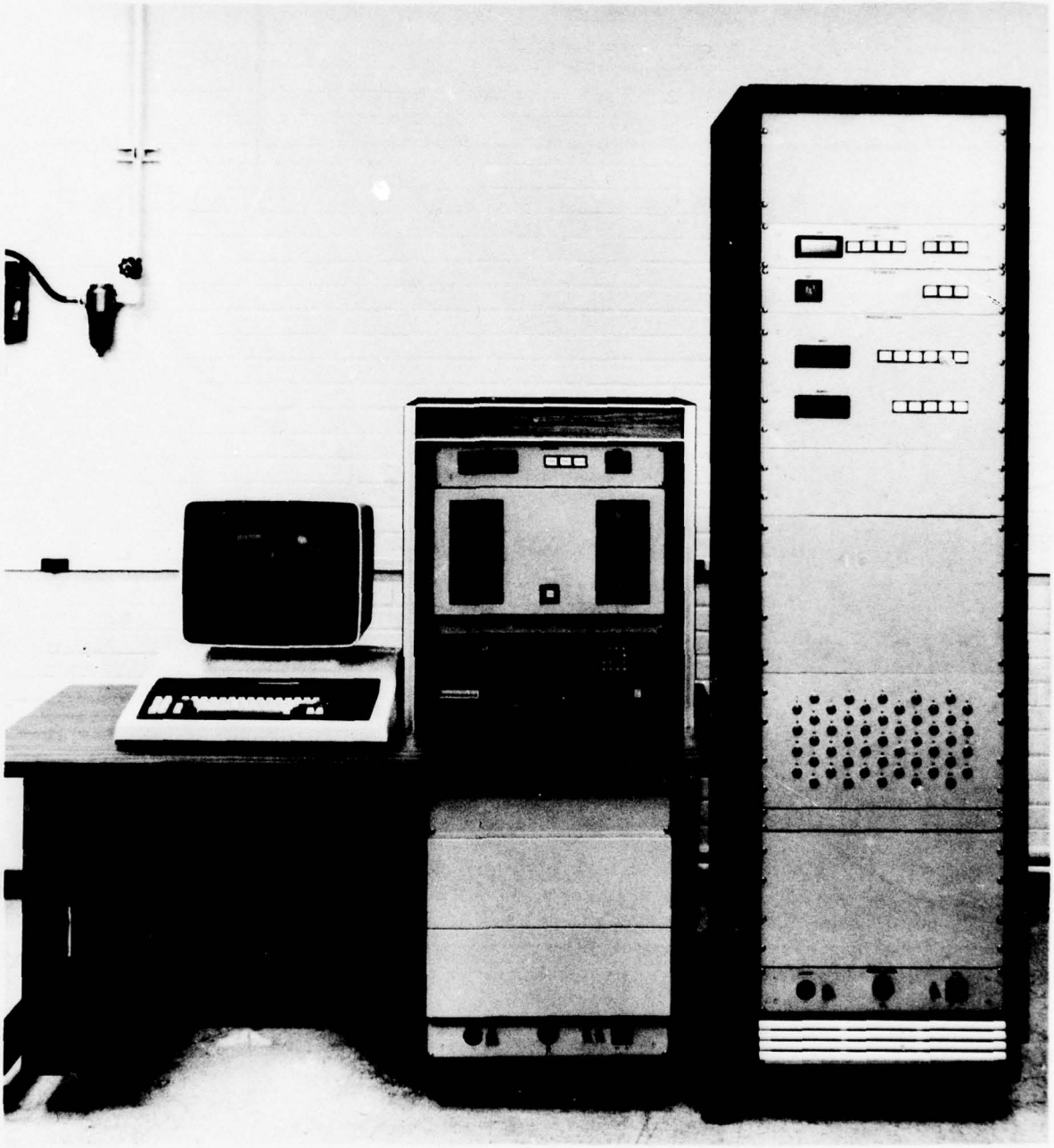

Figure 11. UTRC Boundary Layer Wind Tunnel Data Acquisition System

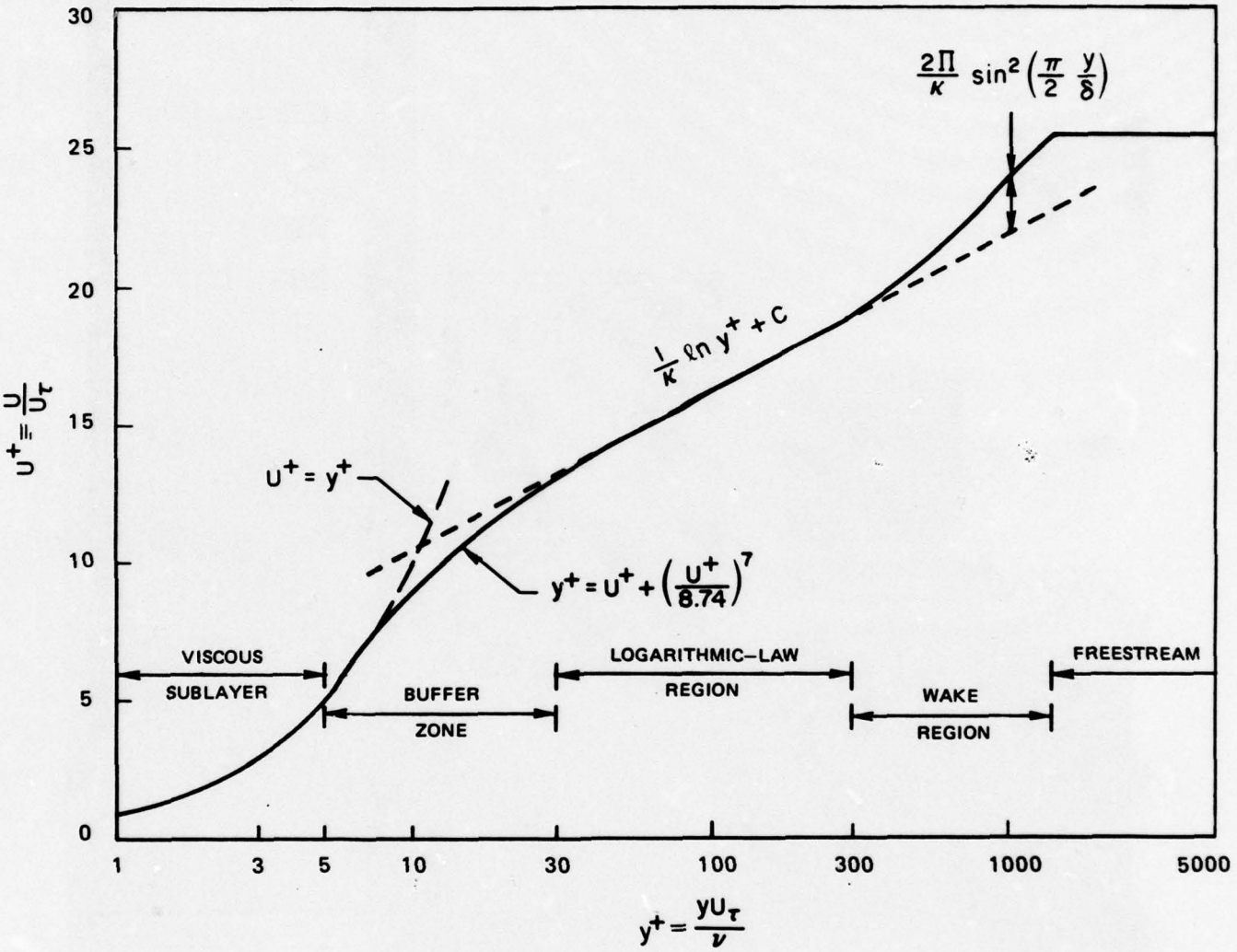

Figure 12. The Universal Velocity Distribution for Constant Pressure Turbulent Boundary Layers

78–12–101–1

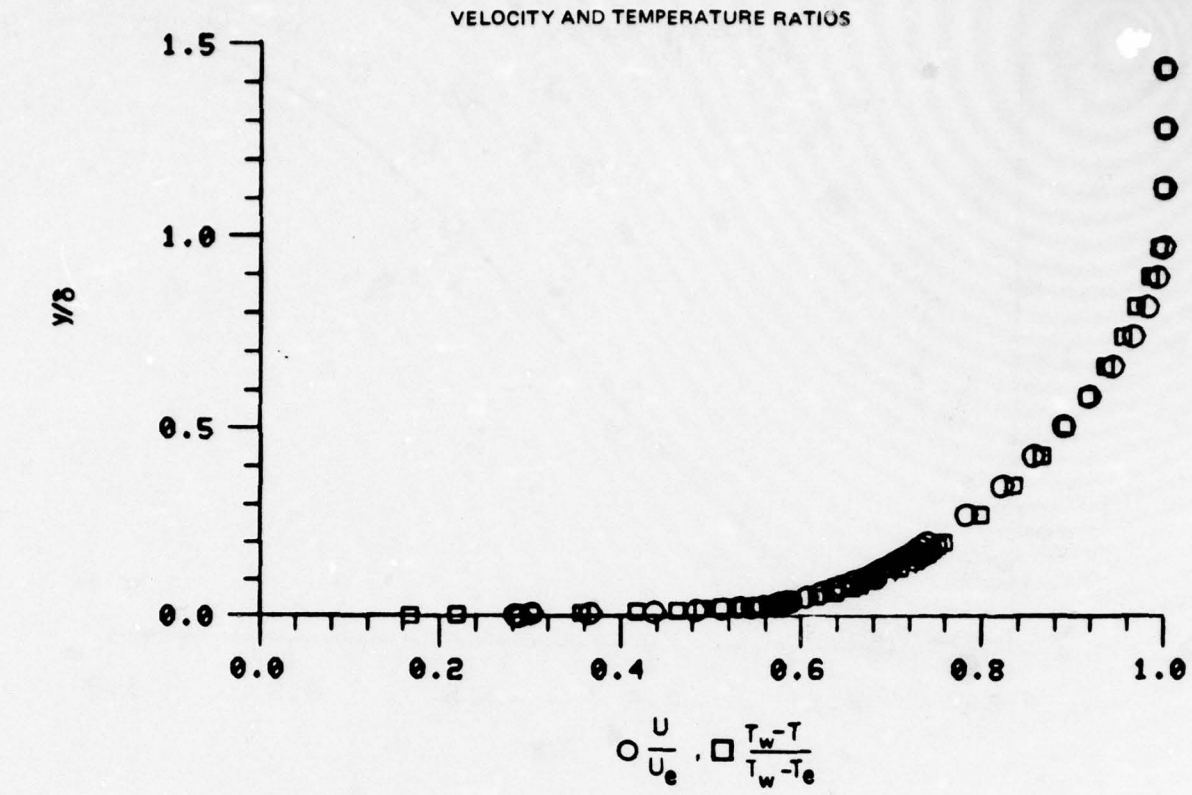

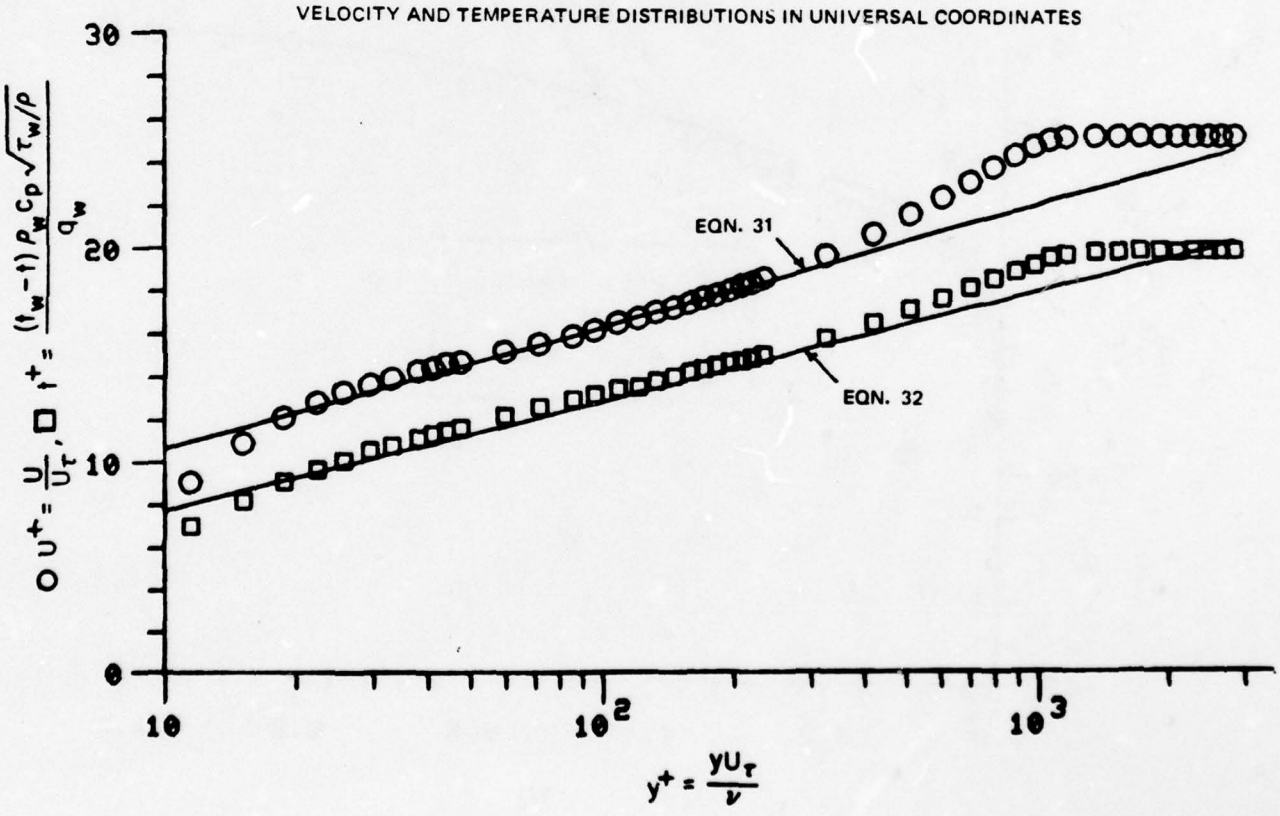

Figure 13A. Typical Boundary Layer Velocity and Temperature Profiles

78-12-100-1

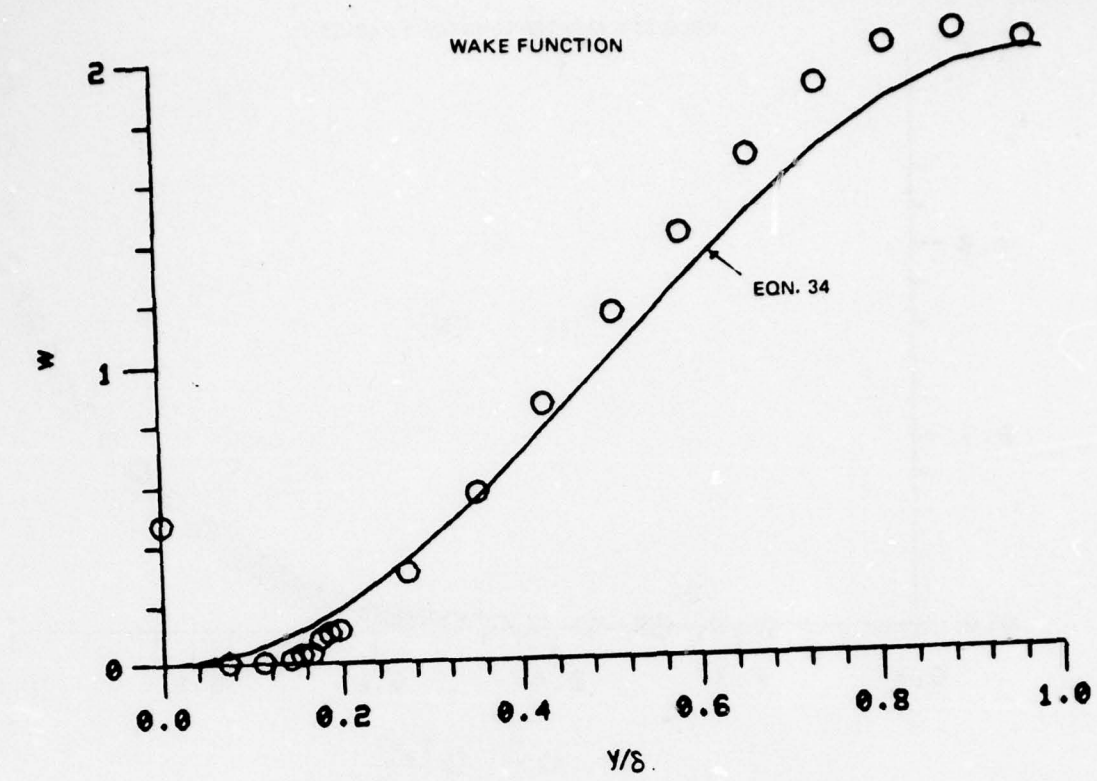

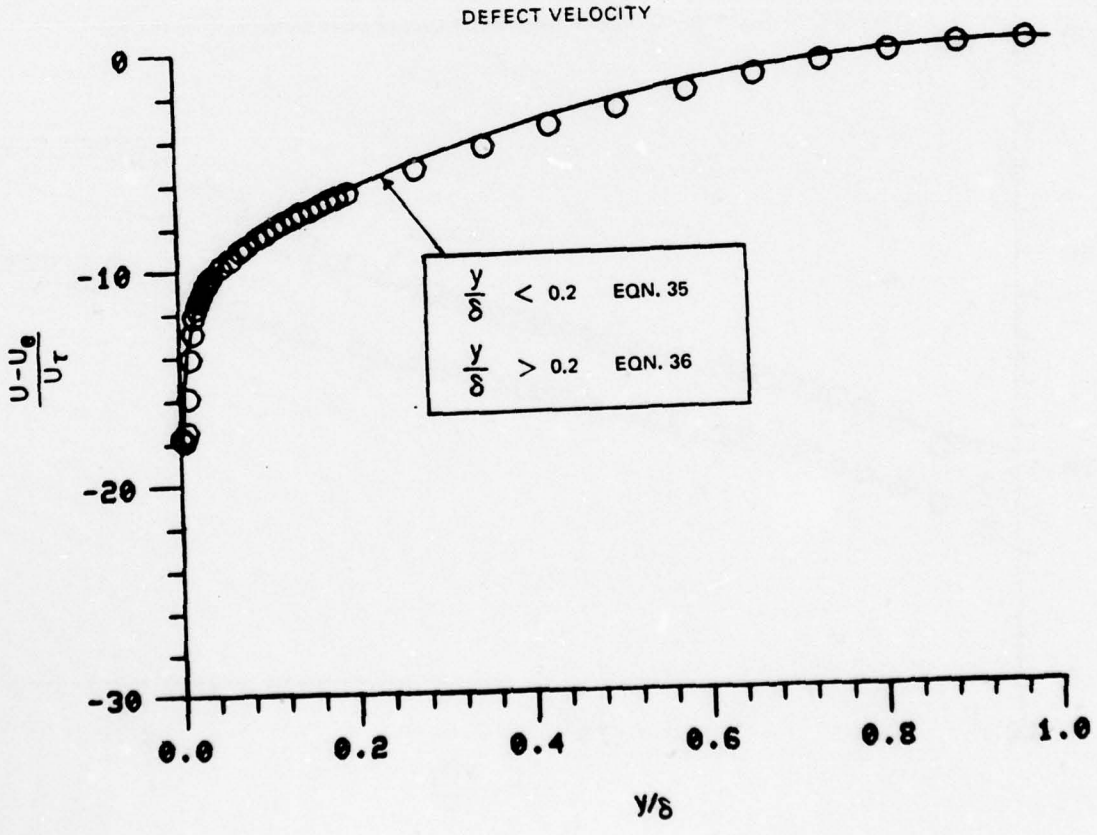

Figure 13B. Typical Boundary Layer Velocity Profiles

78-12-100-2

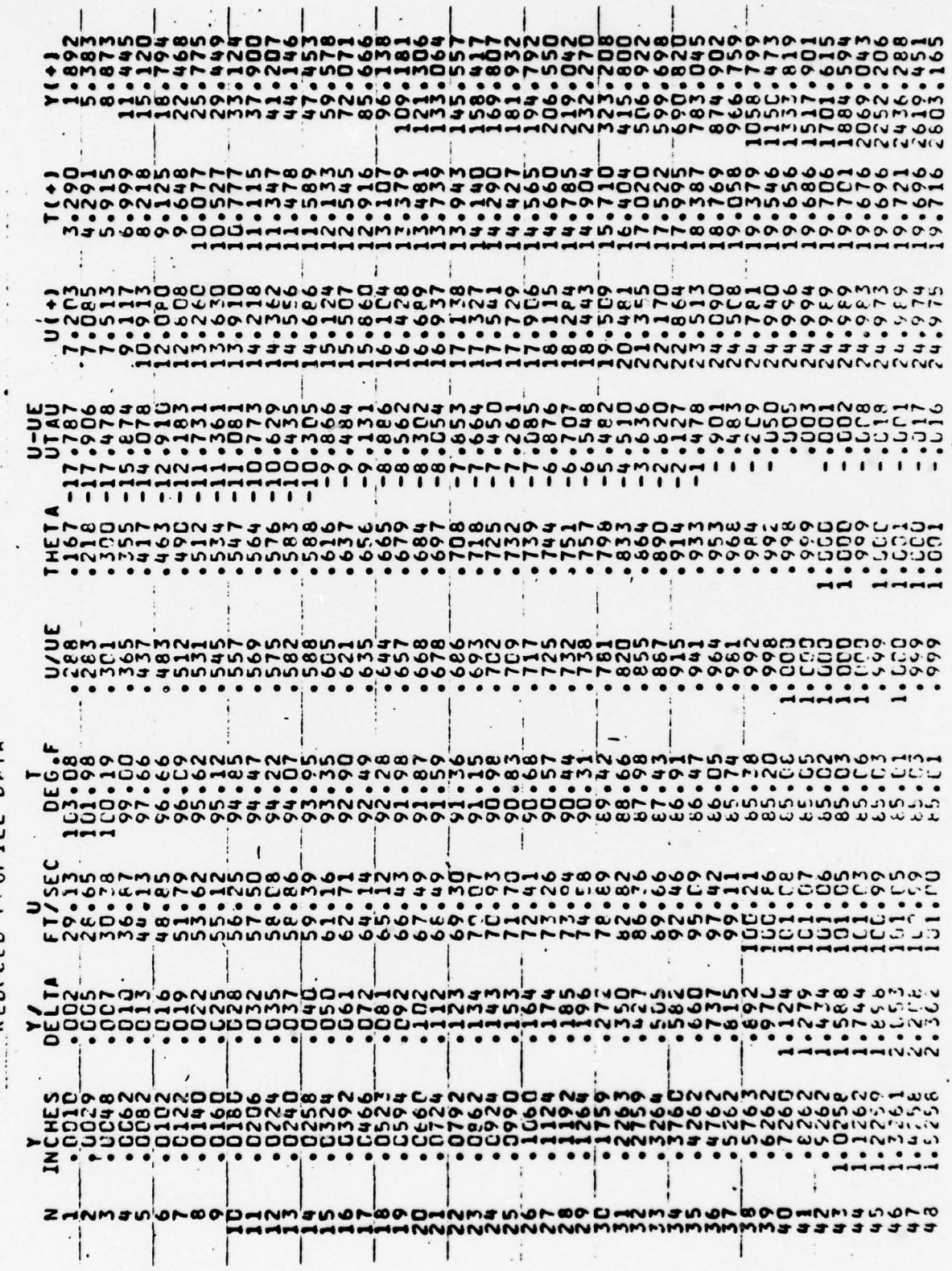

Figure 14. Typical Tabulated Velocity and Temperature Profile Data

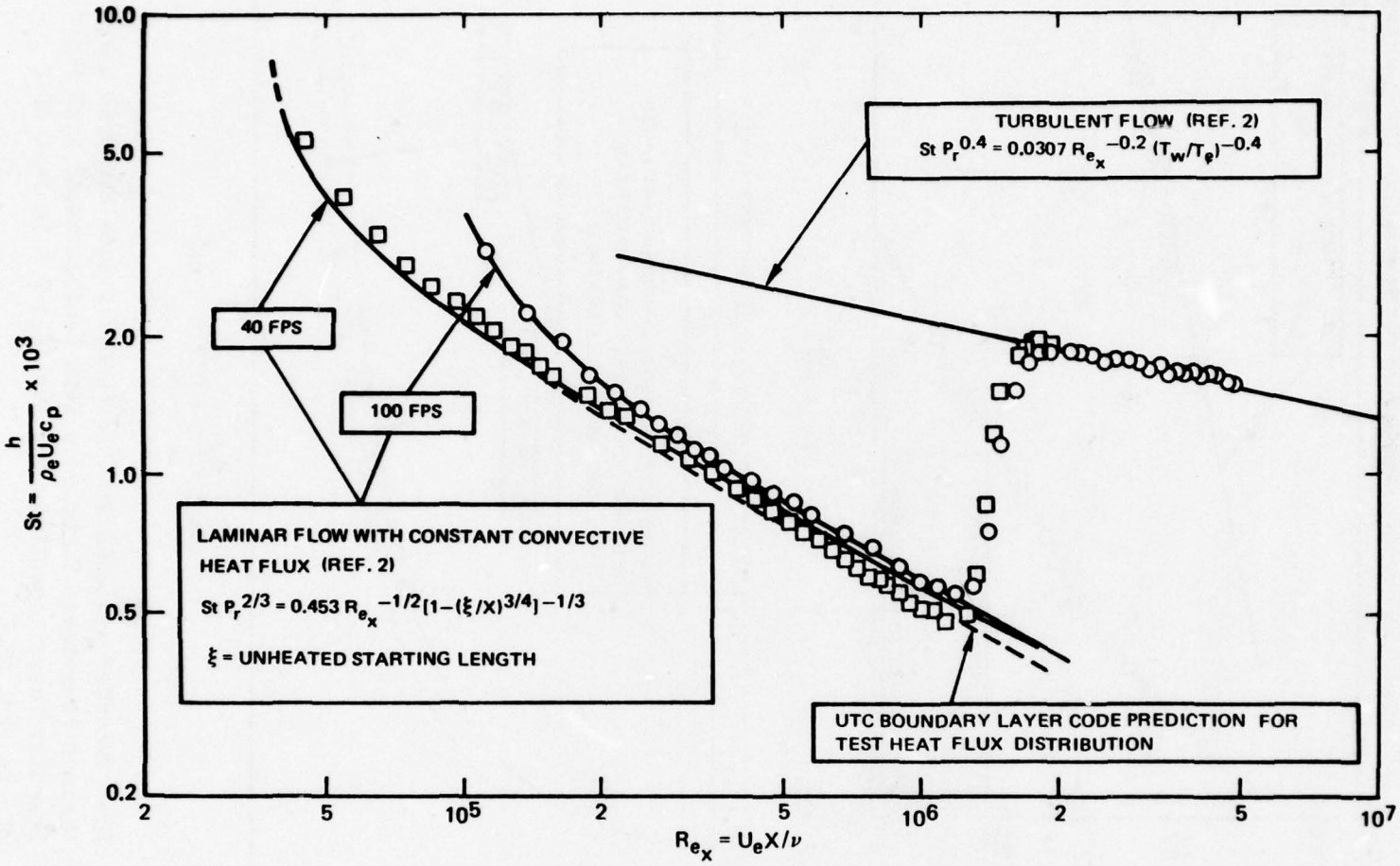

Figure 15. Heat Transfer Distribution Along the Uniform Heat Flux Test Wall For The Minimum Freestream Turbulence Configuration and Natural Transition of the Test Wall Boundary Layer

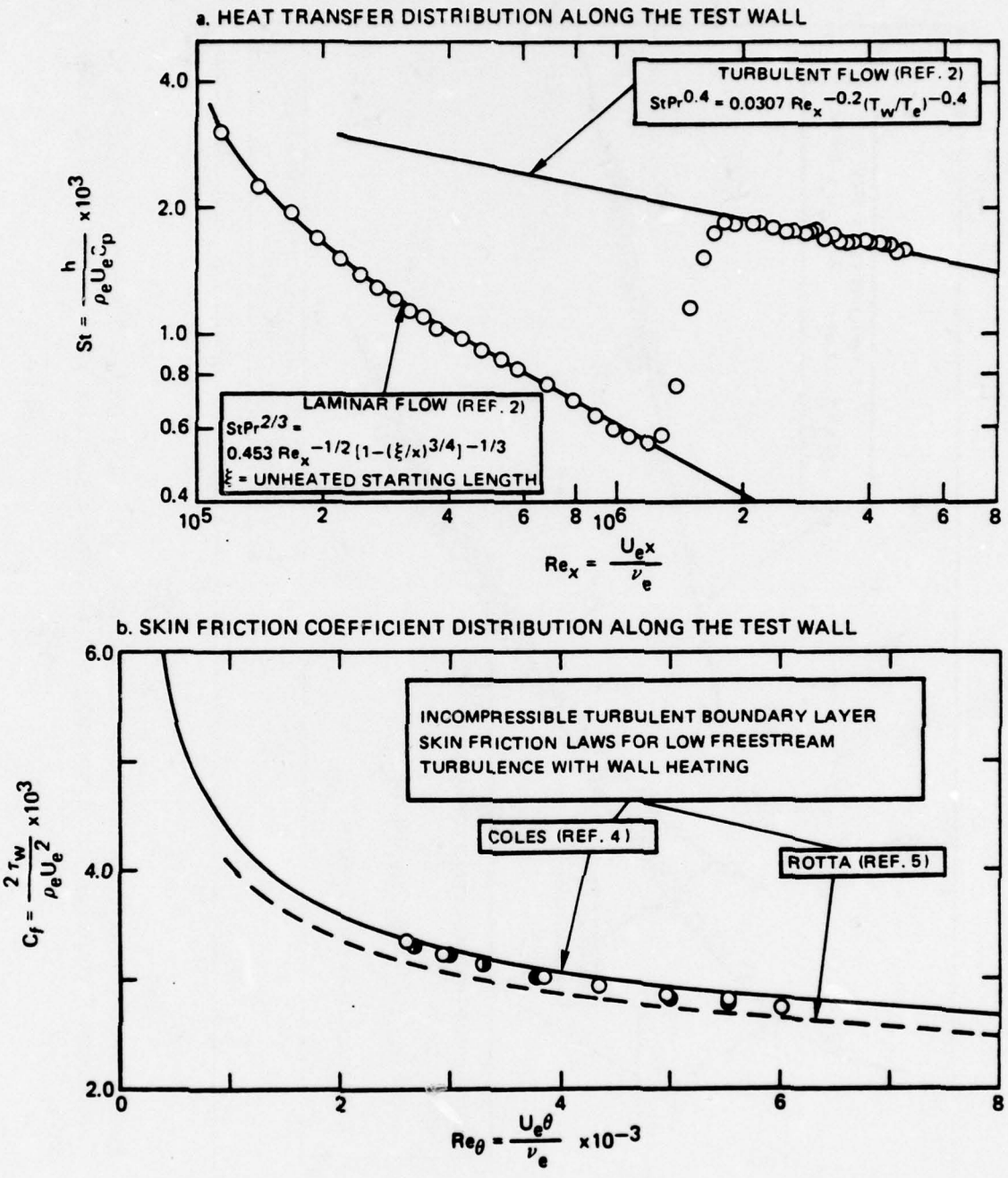

Figure 16. Heat Transfer and Skin Friction Coefficients Measured for the Minimum Freestream Turbulence Test Configuration with Natural Boundary Layer Transition O Tunnel C_L; ● 6 in East of C_L; ◐ 6 in West of C_L

79-05-70-18

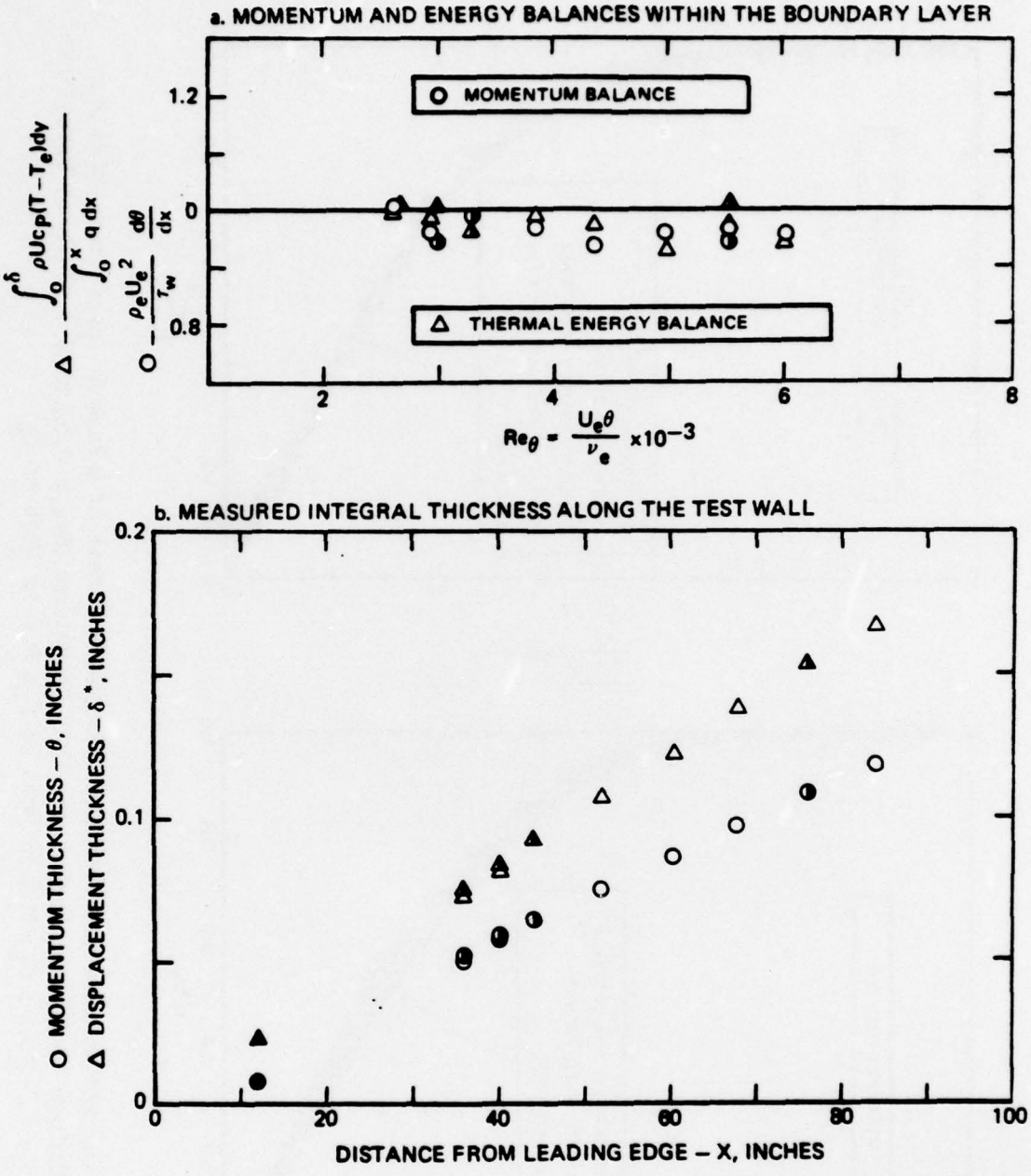

Figure 17. Boundary Layer Properties Measured for the Minimum Freestream Turbulence Test Configuration and Natural Transition of the Test Wall Boundary Layer
O Tunnel C_L; ● 6 in East of C_L; ◐ 6 in West of C_L

79-05-70-12

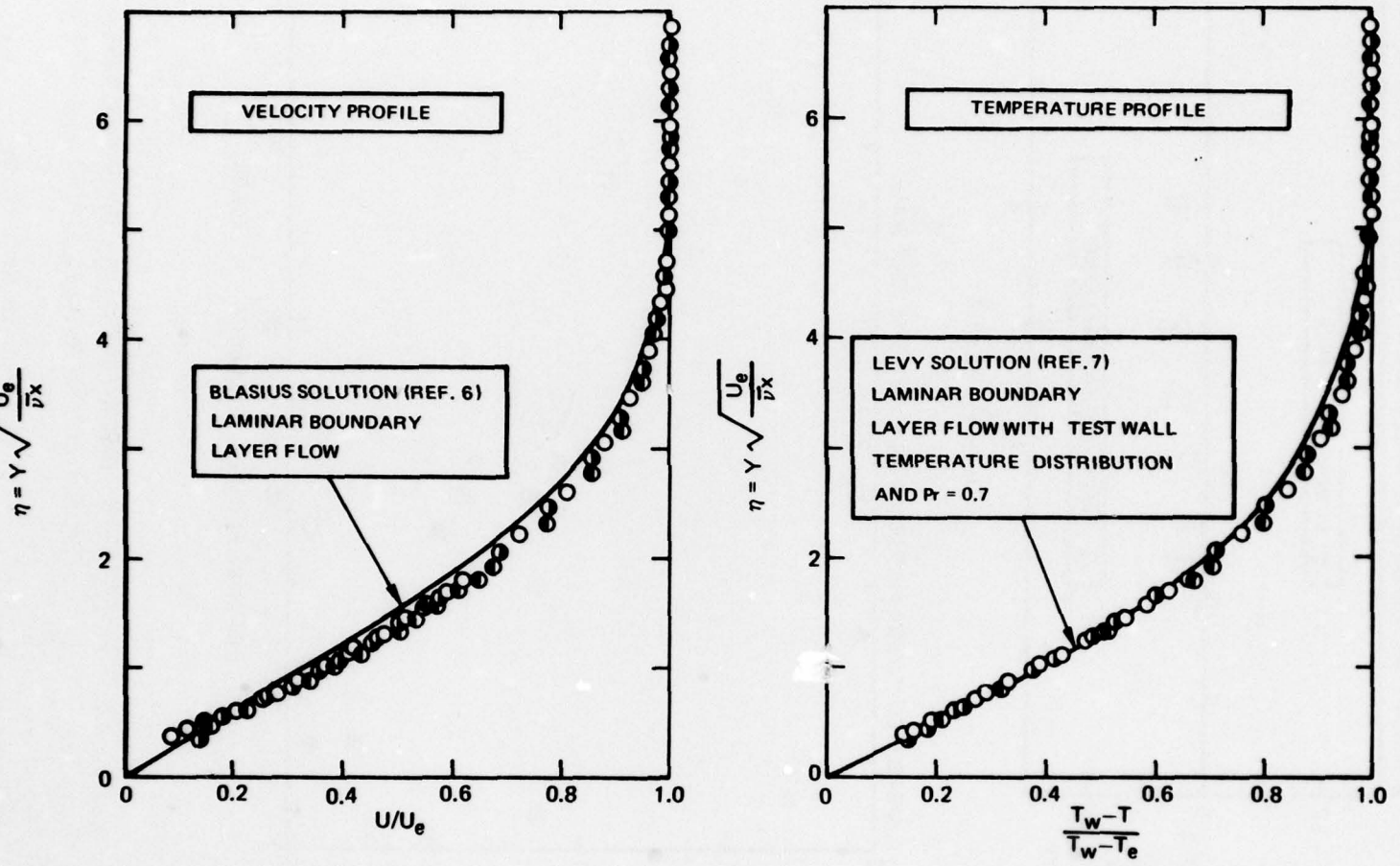

Figure 18. Velocity and Temperature Profiles Measured Upstream of Boundary Layer Transition For The Minimum Freestream Turbulence Test Condition ($Re_x = 0.63 \times 10^6$) at Three Transverse Locations O Tunnel C_L; ◑ 6 in East of C_L; ◐ 6 in West of C_L

79-05-70-6

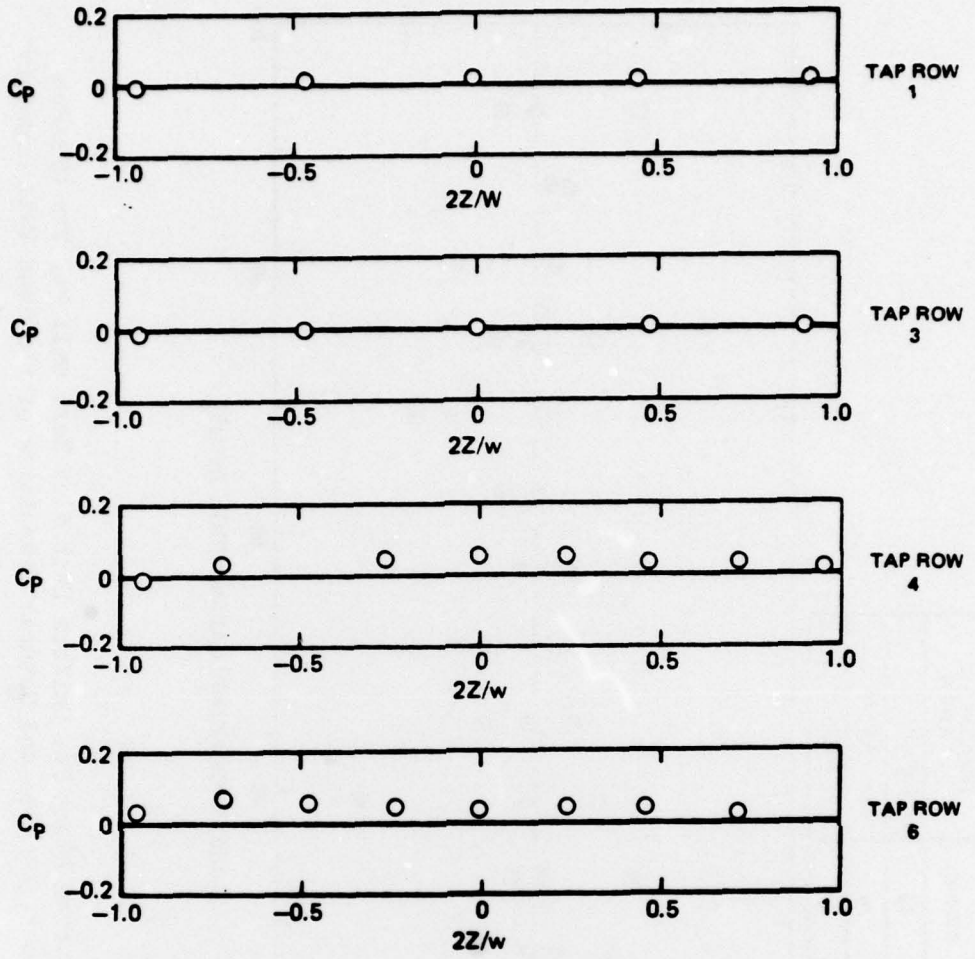

Figure 19. Transverse Distribution of Static Pressure along the Test Wall Leading Edge Bleed Scoop for the Minimum Freestream Turbulence Configuration and Natural Transition of the Test Wall Boundary Layer

79-05-70-9

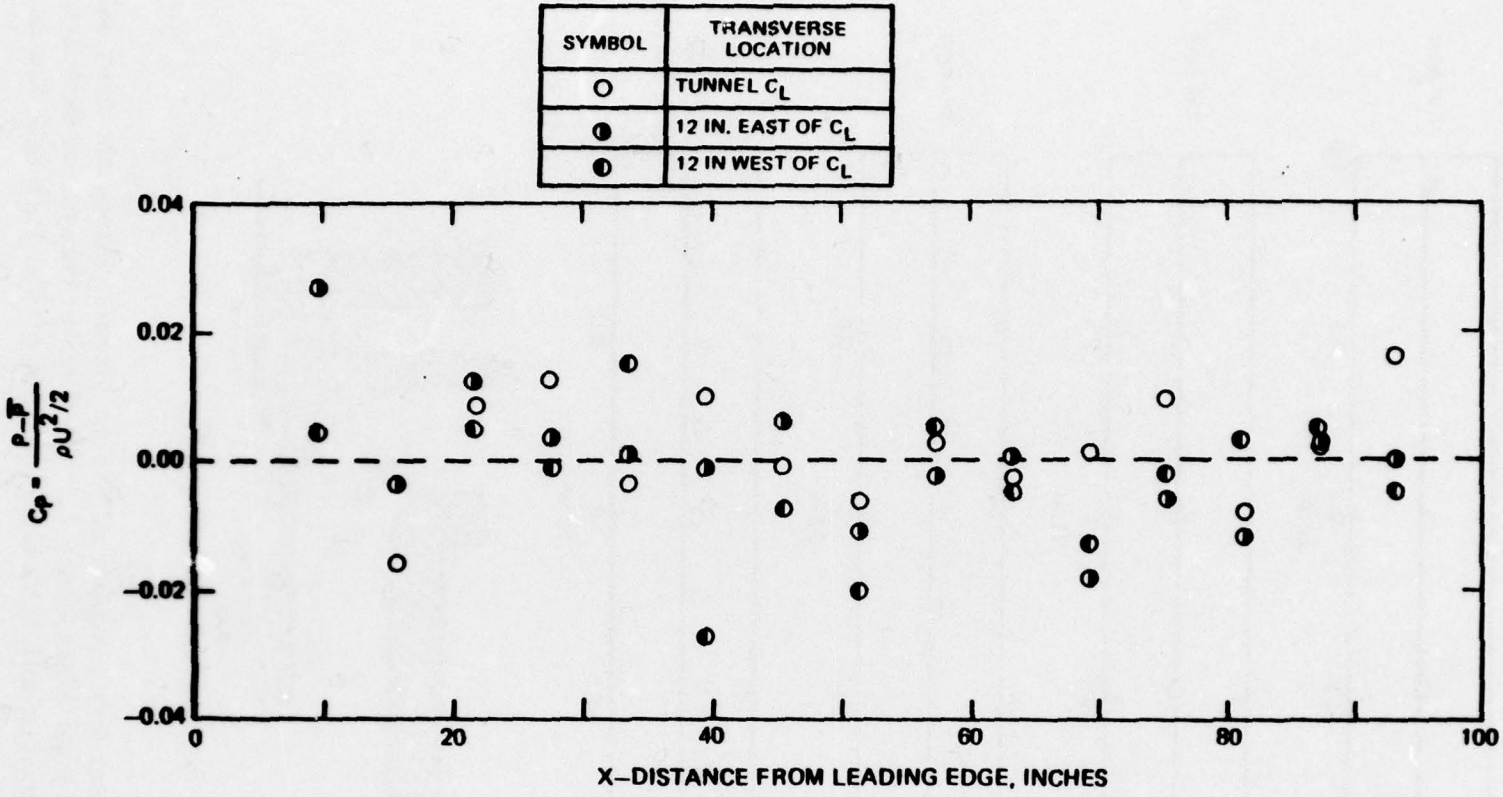

Figure 20. Static Pressure Distribution Along The Uniform Heat Flux Test Wall For The Minimum Freestream Turbulence Configuration and Natural Transition of the Test Wall Boundary Layer

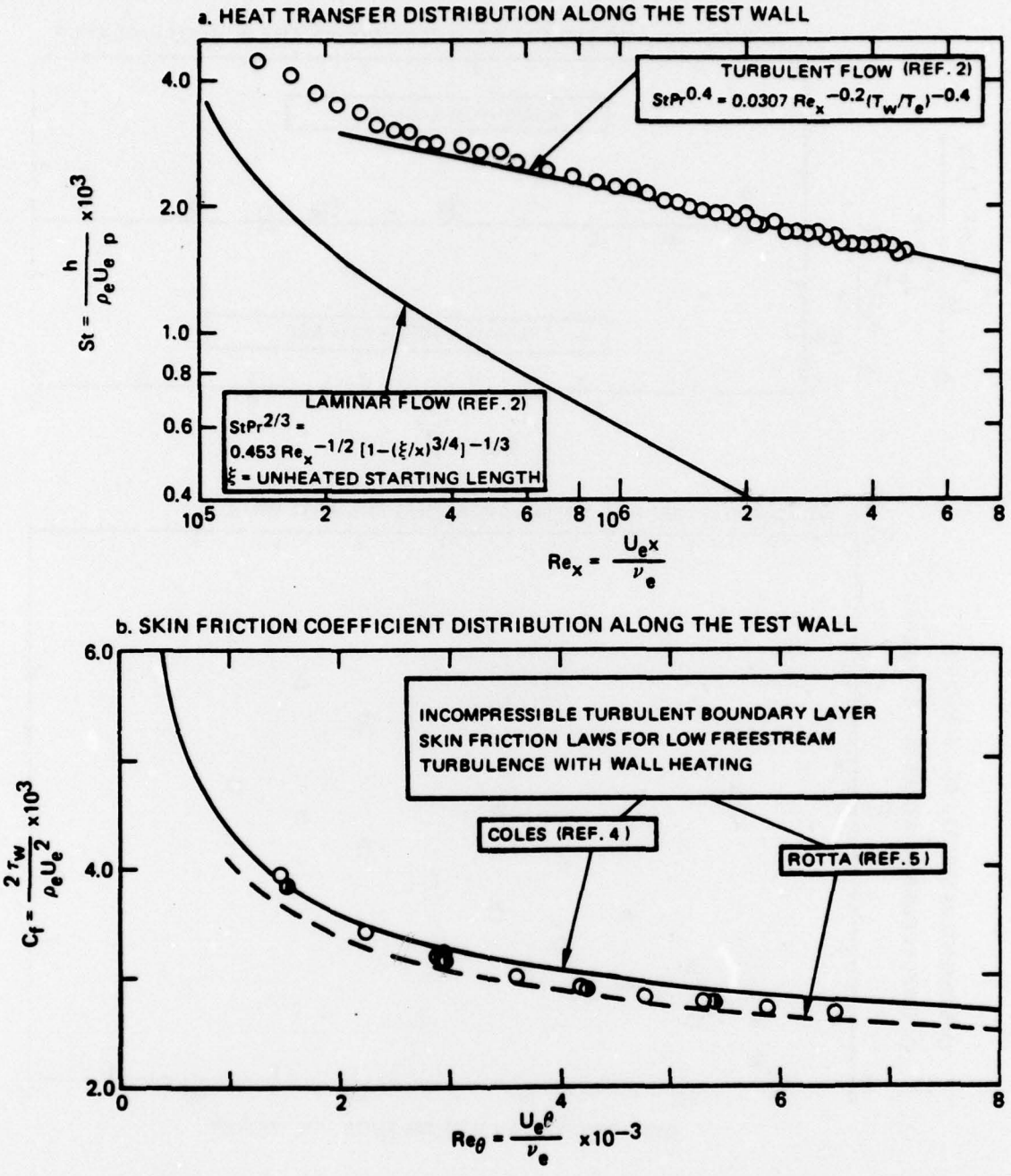

Figure 21. Heat Transfer and Skin Friction Coefficients Measured for the Minimum Freestream Turbulence Test Configuration with the Boundary Layer Trip in Place O Tunnel C_L; ● 6 in East of C_L; ◐ 6 in West of C_L

79-05-70-17

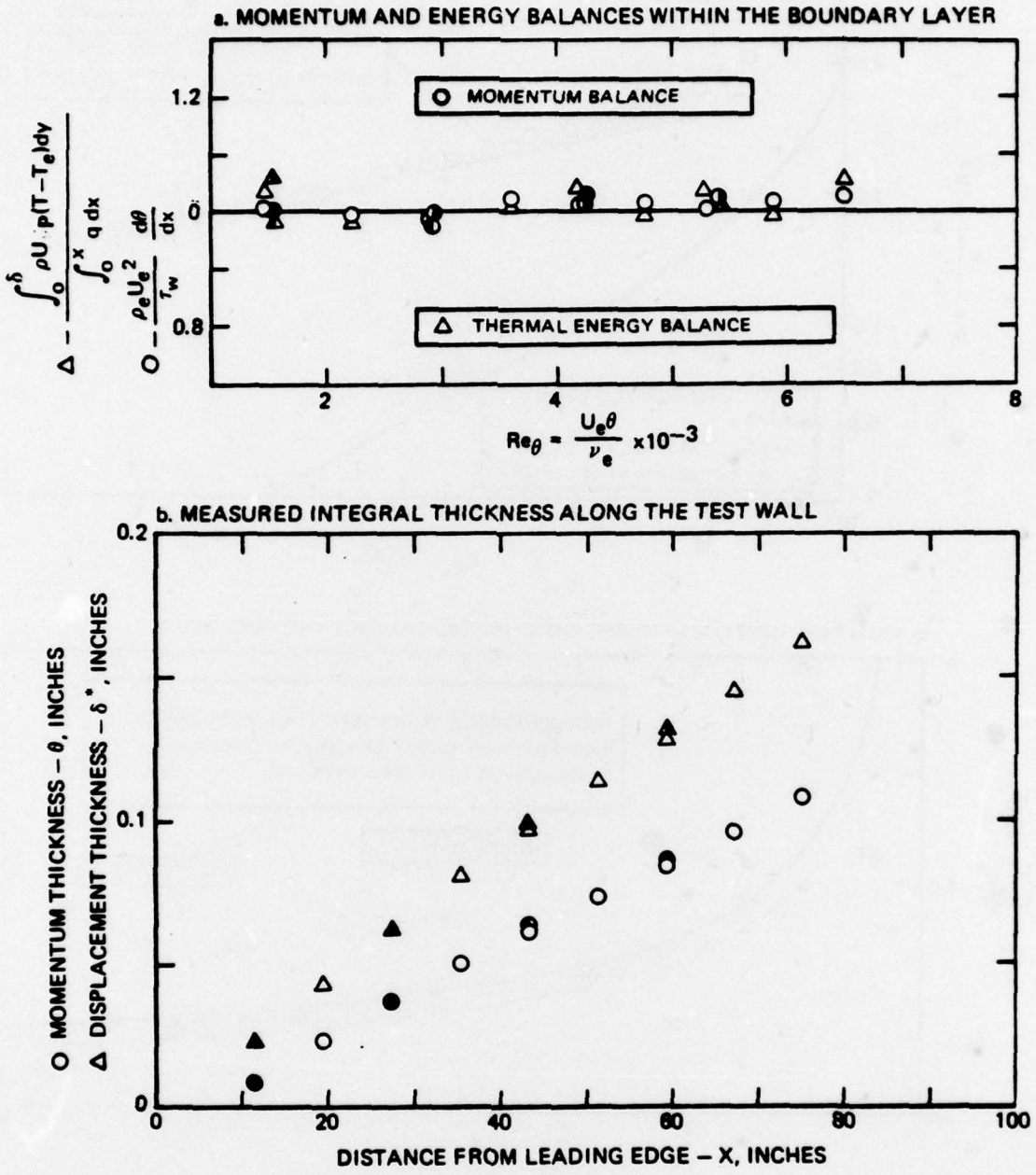

Figure 22. Boundary Layer Properties Measured for the Minimum Freestream Turbulence Test Configuration with the Boundary Layer Trip in Place O Tunnel C_L; ◐ 6 in East of C_L; ◐ 6 in West of C_L

79-05-70-11

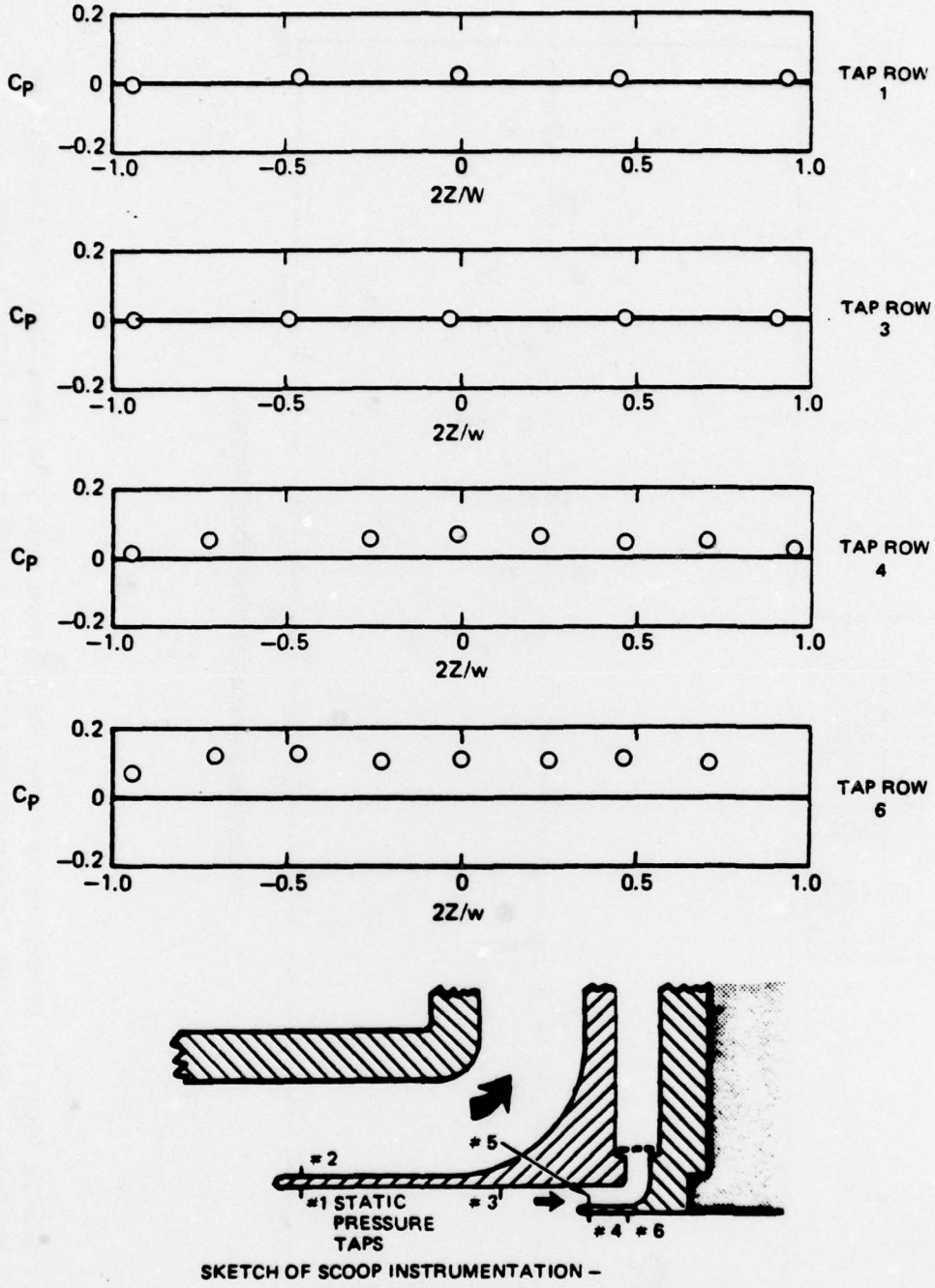

Figure 23. Transverse Distribution of Static Pressure Along the Test Wall Leading Edge Bleed Scoop for the Minimum Freestream Turbulence Configuration and the Boundary Layer Trip in Place

79-05-70-8

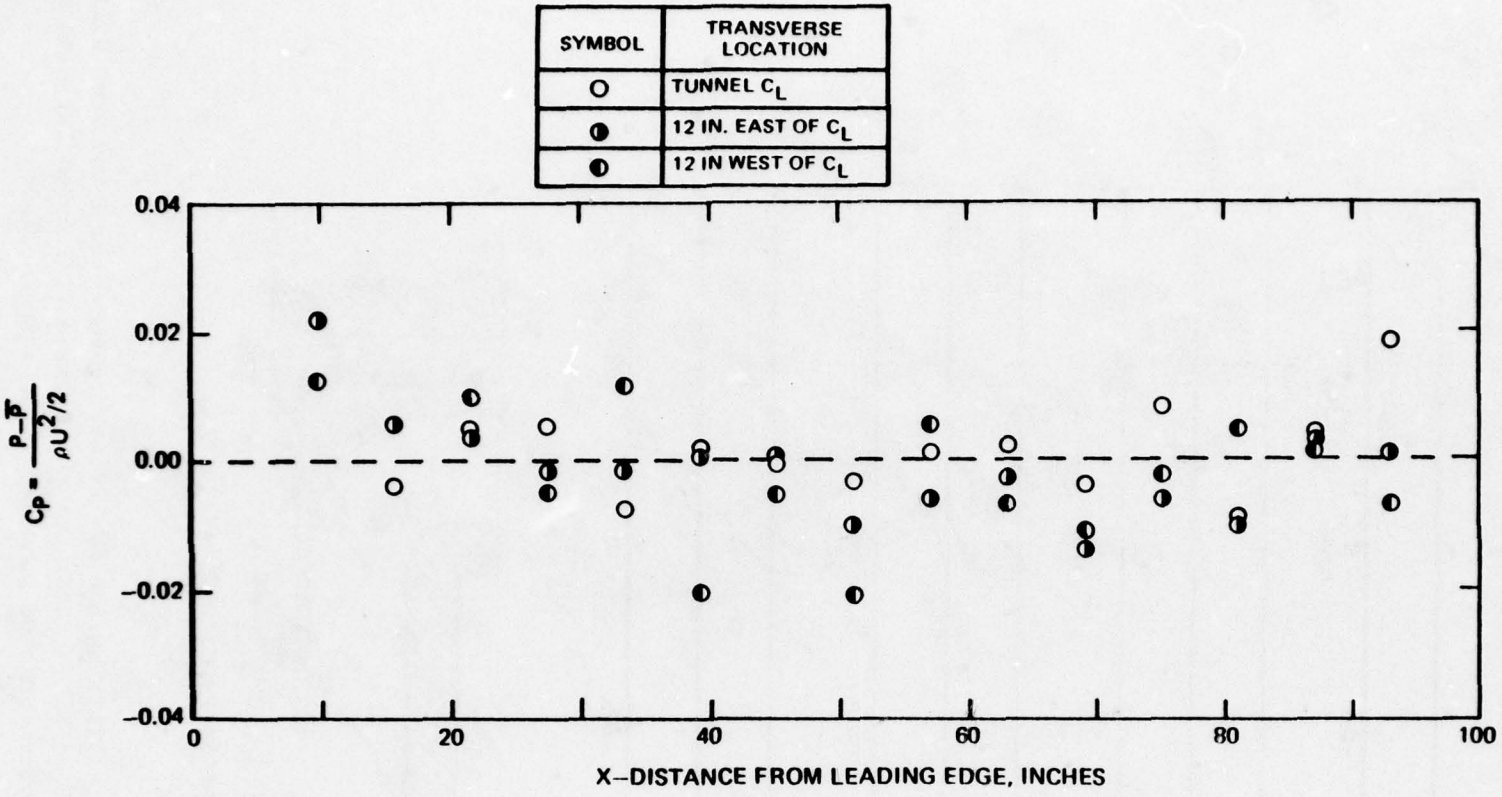

Figure 24. Static Pressure Distribution Along the Uniform Heat Flux Test Wall For the Minimum Freestream Turbulence Configuration with the Boundary Layer Trip in Place

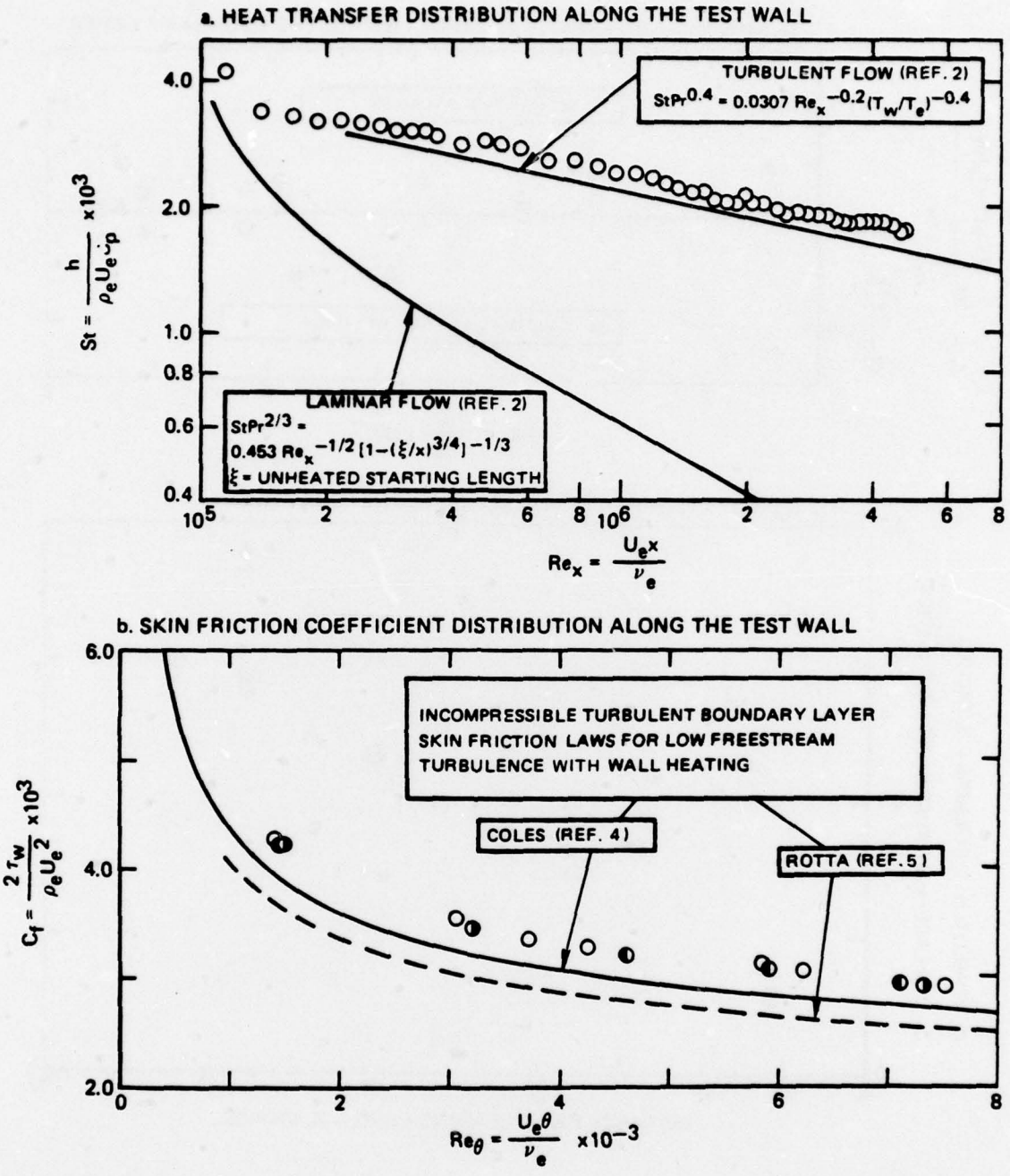

Figure 25. Heat Transfer and Skin Friction Coefficients Measured With Turbulence Generating Grid Number 3 Installed
○ Tunnel C_L; ◑ 6 in East of C_L; ◐ 6 in West of C_L

79-05-70-19

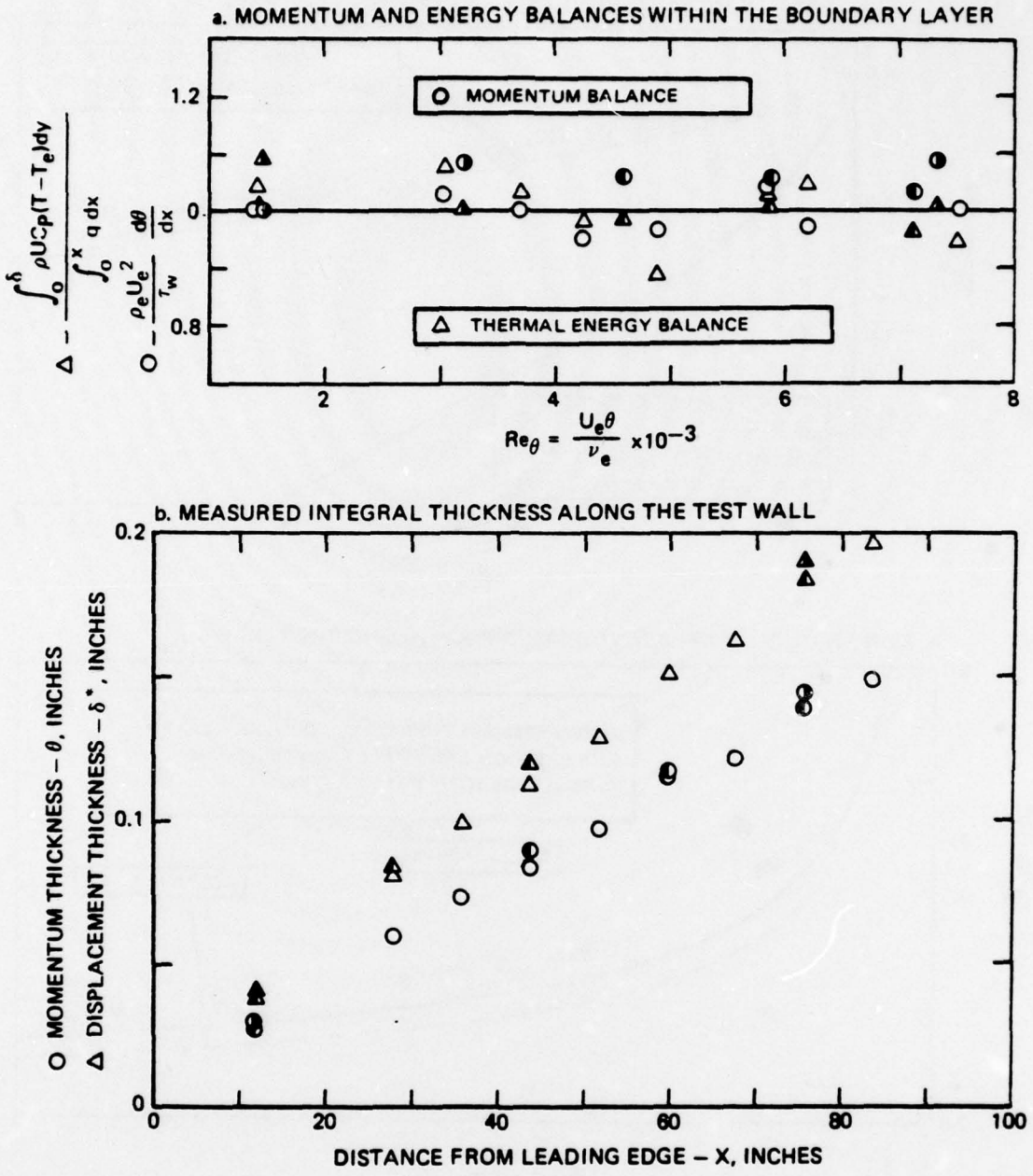

Figure 26. Boundary Layer Properties Measured with Turbulence Generating Grid Number 3 Installed
O Tunnel C_L; ◐ 6 in East of C_L; ◑ 6 in West of C_L

79-05-70-13

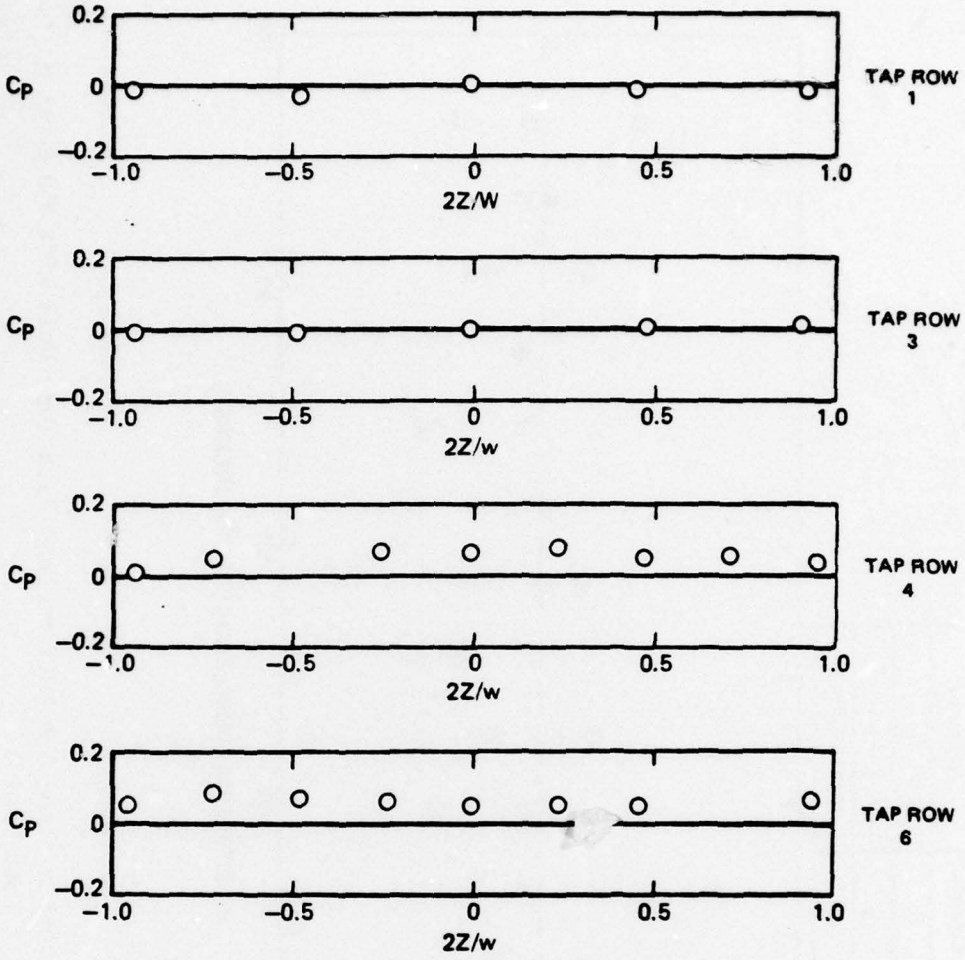

Figure 27. Transverse Distribution of Static Pressure along the Test Wall Leading Edge Bleed Scoop with Turbulence Generating Grid Number 3 Installed

79-05-70-10

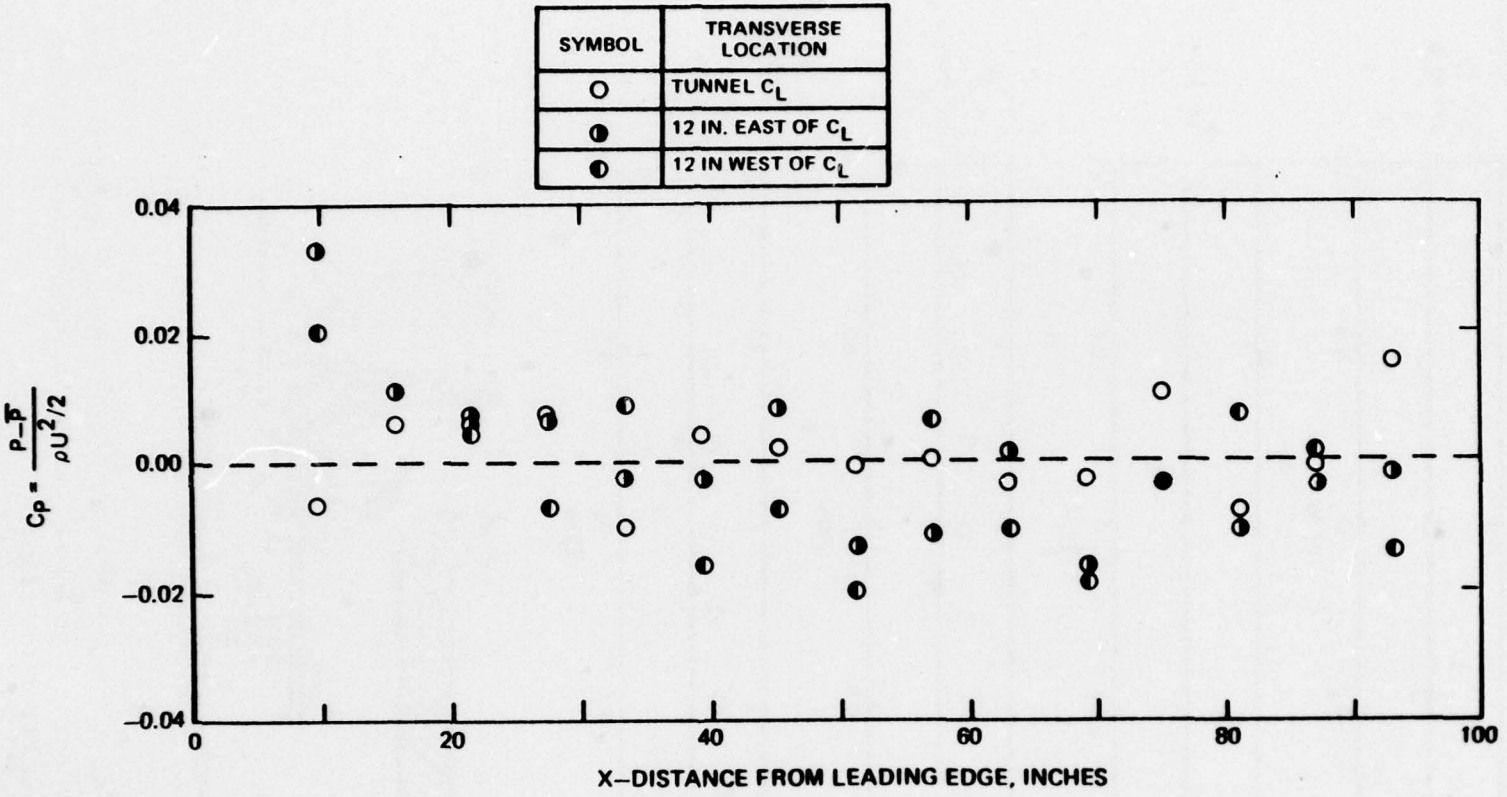

Figure 28. Static Pressure Distribution Along the Uniform Heat Flux Test Wall with Turbulence Generating Grid Number 3 Installed

LIST OF WRITTEN PUBLICATIONS

The research performed under this contract has not yet progressed to the point where journal articles can be written.

LIST OF PROFESSIONAL PERSONNEL ASSOCIATED WITH THE RESEARCH EFFORT

Blair, Michael F. - Research Engineer, Gas Turbine Technology Group, Gas Dynamics Section
- Principal Investigator and Project Manager

Dring, Robert P. - Supervisor, Gas Turbine Technology Group, Gas Dynamics Section

Werle, Michael J. - Section Chief, Gas Dynamics Section

INTERACTIONS

a. Spoken Papers - no spoken papers were delivered on this contract research.

b. Consultive and Advisory functions - Discussions have been held with Professor David Walker of Lehigh University concerning the use of a turbulent boundary layer/pressure gradient data analysis developed by him. Professor Walkers' data analysis system was developed under AFOSR funding and reported in Ref. 27. The data analysis system will be employed for this present research contract for those boundary layer profile data obtained in streamwise pressure gradients.

LIST OF NEW DISCOVERIES OR PATENTS

The research performed under the present contract has not yet progressed to a point where specific new discoveries have been defined. No patents have resulted from any work conducted under this contract.

Unclassified

SECURITY CLASSIFICATION OF THIS PAGE (When Data Entered)

REPORT DOCUMENTATION PAGE	READ INSTRUCTIONS BEFORE COMPLETING FORM
1. REPORT NUMBER: AFOSR-TR- 79-0936	2. GOVT ACCESSION NO. / 3. RECIPIENT'S CATALOG NUMBER
4. TITLE (and Subtitle): AN EXPERIMENTAL AND ANALYTICAL STUDY OF BOUNDARY LAYERS IN HIGHLY TURBULENT FREESTREAMS	5. TYPE OF REPORT & PERIOD COVERED: INTERIM; 1 Jun 78 - 1 Jun 79
	6. PERFORMING ORG. REPORT NUMBER: R78-914388-5
7. AUTHOR(s): M F BLAIR	8. CONTRACT OR GRANT NUMBER(s): F49620-78-C-0064
9. PERFORMING ORGANIZATION NAME AND ADDRESS: UNITED TECHNOLOGIES RESEARCH CENTER, SILVER LANE, EAST HARTFORD, CT 06108	10. PROGRAM ELEMENT, PROJECT, TASK AREA & WORK UNIT NUMBERS: 2307A4; 61102F
11. CONTROLLING OFFICE NAME AND ADDRESS: AIR FORCE OFFICE OF SCIENTIFIC RESEARCH/NA, BLDG 410, BOLLING AIR FORCE BASE, D C 20332	12. REPORT DATE: July 1979
	13. NUMBER OF PAGES: 69
14. MONITORING AGENCY NAME & ADDRESS(if different from Controlling Office)	15. SECURITY CLASS. (of this report): UNCLASSIFIED
	15a. DECLASSIFICATION/DOWNGRADING SCHEDULE

16. DISTRIBUTION STATEMENT (of this Report)

Approved for public release; distribution unlimited.

17. DISTRIBUTION STATEMENT (of the abstract entered in Block 20, if different from Report)

18. SUPPLEMENTARY NOTES

19. KEY WORDS (Continue on reverse side if necessary and identify by block number)

TURBULENT BOUNDARY LAYERS
FREE-STREAM TURBULENCE
TRANSITION
HEAT TRANSFER
BOUNDARY LAYER PROFILES

20. ABSTRACT (Continue on reverse side if necessary and identify by block number)

During the first year of the contract period experimental research has been conducted to determine the influence of free-stream turbulence on zero pressure gradient, incompressible, fully turbulent boundary layer flow. During this period convective heat transfer coefficients, boundary layer mean velocity and temperature profile and wall static pressure distribution data were obtained for two flow conditions of constant free-stream velocity and low free-stream turbulence intensity and for flow condition of constant free-stream velocity and higher free-stream turbulence. Documentation of the free-stream turbulence for these flows

DD FORM 1 JAN 73 1473

UNCLASSIFIED

SECURITY CLASSIFICATION OF THIS PAGE (When Data Entered)

is currently in progress. The conclusion reached from the low free-stream turbulence test results is that these data are in excellent agreement with classic two-dimensional, low free-stream turbulence, turbulent boundary layer correlations, thus establishing the absolute accuracy of the experiment. The data obtained for the higher free-stream turbulence test case indicates that free-stream turbulence does have a significant effect on fully turbulent boundary layer skin friction and heat transfer. A quantitative assessment of this influence will emerge as data is obtained for additional free-stream turbulence levels and as the turbulence distributions are documented. The data obtained during this first year of the contract effort constitute part of task "a" of the Statement of Work of the subject contract.